SLAC-PUB-16406
September 2015

COLLECTIVE EFFECTS IN A DIFFRACTION-LIMITED STORAGE RING*

Ryutaro Nagaoka
Synchrotron SOLEIL, L'Orme des Merisiers, 91190 Saint-Aubin, France
Karl L. F. Bane
SLAC National Accelerator Laboratory, Stanford, CA 94309, USA

Published in Journal of Synchrotron Radiation, Volume 21, Part 5, September 2014

* Work supported in part by the Department of Energy, Office of Science, Office of Basic Energy Science, under Contract No. DE-AC02-76SF00515.

Collective Effects in a Diffraction Limited Storage Ring

Authors

Ryutaro Nagaoka* and Karl L.F. Bane

Correspondence email: nagaoka@synchrotron-soleil.fr

Synopsis An overview of beam collective effects in DLSRs is given. The relation of a very low emittance machine and its stored beam to the former is described.

Abstract This paper gives an overview of collective effects that are likely to appear and possibly limit the performance in a DLSR that stores a high intensity ultra-low emittance beam. We aim to cover beam instabilities and other intensity-dependent effects that may significantly impact the machine performance. The latter include beam-induced machine heating, Touschek scattering, IBS (Intra Beam Scattering), as well as incoherent tune shifts. The general trend that the efforts to achieve ultra-low emittance result in increasing the machine coupling impedance and the beam sensitivity to instability is reviewed. The nature of coupling impedance in a DLSR is described, followed by a series of potentially dangerous beam instabilities driven by the former, such as resistive-wall, TMCI (Transverse Mode Coupling Instability), head-tail and microwave instabilities. In addition, beam-ion instability and CSR instability are also treated. Means to fight against collective effects such as, lengthening of the bunch with passive harmonic cavities and bunch by bunch transverse feedback are introduced. Numerical codes developed and used to evaluate the machine coupling impedance, as well as to simulate beam instability using the former as inputs are described.

1. Introduction

Since the advent of material science in the early 1970s that made parasitic use of the synchrotron radiation from dipole magnets in electron storage rings built for high energy physics experiments, there has been a continuing explosive evolution in the development of electron storage rings built as dedicated sources of synchrotron radiation. While the so called first generation light sources consist of those utilised parasitically as mentioned above, the second generation rings are those built dedicatedly as synchrotron radiation sources, but still using the light from bending magnets, and the third generation machines are referred to as those using insertion devices as the primary radiation sources. A large number of third generation light source rings (LSRs) have been built worldwide since the 1990s up to the early 2010s. Not only did these 3rd generation LSRs differ from the former in the use of insertion devices, but their performance markedly improved in terms of the brilliance of the synchrotron radiation.

The brilliance, as is well known, scales inversely proportional to the two transverse emittances of the electron beam and linearly proportional to the electron beam intensity. Namely, there are two major axes in raising the brilliance of an electron storage ring: Lowering the transverse emittances and increasing the beam intensity. Large efforts have therefore been made to construct low emittance rings through a number of different magnet lattice designs. In parallel, efforts have been made to increase the beam intensity, where up above a certain current the beam becomes collectively unstable due to its self EM field, called a wake field, acting back on itself. As in other types of storage rings such as colliders for high energy physics experiments, in which the event of particle collision depends linearly on the beam intensity, the study of collective instability has been of great importance in LSRs in reaching higher brilliance. While the majority of synchrotron radiation users request a high average photon flux, and therefore, a high average electron beam current, there are also those carrying out time-resolved experiments utilising the strict timing of electron bunches circulating in a ring. In order to increase the brilliance for such experiments, one needs to correspondingly increase the bunch intensity. A high intensity bunch is sensitive to short-range wake fields that are excited by the bunch itself and drive the so called single bunch instabilities, while a high intensity multibunch beam is subject to long-lasting wakes excited by the ensemble of bunches and induce coupled-bunch instabilities. To increase the brilliance of a storage-ring based light source with beam intensity, therefore, collective beam instability of both single and multibunch must be studied along with wake fields, of short- and long-range nature, which drive the former respectively.

After nearly two decades of time during which, a large number of 3rd generation light sources were constructed and operated around the world as mentioned already, most of which having the horizontal emittance in a few nanometer range, yet a newer generation of storage ring light sources, named as DLSRs (Diffracted Limited Storage Rings), have begun to emerge in the last years. To be diffraction limited in the horizontal plane in the photon energy range of interest, the horizontal emittance is roughly one order of magnitude lower than the 3rd generation light sources, namely in the few hundreds of picometer range or lower. The first such machine would be MAXIV currently under construction in Sweden, followed by Sirius in Brazil. In addition to the former, there are plans to convert the existing 3rd generation machines into DLSRs, such as ESRF-II, APS-II and SPring-8. This major performance upgrade of the storage rings came out to be feasible thanks to a marked progress made particularly in the magnet technology enabling a compact magnet lattice design with extremely high gradient fields, as well as gained operational experiences with 3rd generation light sources. In exploiting such major steps forward in the magnet lattice, it would be a pity if the beam intensity could not be kept at least to its previous levels.

As we shall see below, however, storing a comparable level of beam in a DLSR turns out to be not straightforward. The conditions to keep the beam stable against collective effects will be more stringent for at least two reasons; firstly, due to an increase in the coupling impedance, and secondly

due to enhancement of the beam sensitivity against collective effects. In addition, much smaller transverse beam dimensions significantly enhance intra-beam and Touschek scattering as the beam intensity is increased, making it more and more incompatible to store a high intensity, ultra-low emittance beam. The scope of the present paper is to make an overview of these collective effects in a DLSR.

The paper is organized as follows: In the next section, we shall review the generally inevitable difficulty in an ultra-low emittance lattice design resulting in an increase in the coupling impedance, at the same time enhancing the beam sensitivity against collective instability. In Sec.3 we shall describe the general characteristics of the coupling impedance in a DLSR. Then in Sec.4, we shall go through the beam instabilities that are considered to be potentially dangerous in a DLSR. In Sec. 5, we shall discuss two types of Coulomb scattering, IBS (Intra-Beam Scattering) and Touschek scattering, which become important issues in a DLSR, as they may blow up the transverse emittance and deteriorate the beam lifetime. We shall then see in Sec. 6 other collective effects that may be a concern in a DLSR, which are the beam-induced machine heating and incoherent transverse tune shifts. We shall review several means that are considered effective in alleviating or curing collective effects in a DLSR in Sec. 7. Finally, conclusions shall be given in Sec. 8.

2. DLSRs and their links to collective effects

Before going into specific collective effects in a DLSR, let us start from reviewing the general background of how collective effects may become an important issue in a DLSR. In particular, the ways in which ultralow emittance optics in a DLSR, as well as the machine conditions imposed to realize the former likely enhance collective effects. This correlation may be useful to note in order to have a global vision of the subject.

The starting point is the brightness which is the primary figure of merit of a storage-ring based light source representing its performance. As is well-known, it scales linearly proportional to the beam intensity and inversely proportional to the product of transverse beam sizes and divergences, namely the transverse emittances. The latter explains the continuing effort to minimize the emittance of a storage ring. A DLSR stores an electron beam whose emittances in the two transverse planes are diffraction limited in the photon energy range of interest. The beam intensity, which is proportional to the brightness and therefore constituting the other major axis in increasing the latter, can usually be raised until it is limited by collective effects, the details of which shall be the subject of this paper. Since light sources deliver synchrotron radiation in different ways according to the users' request, such as time-averaged or time-resolved high photon flux, the high electron beam intensity requested may either represent the total beam current or the current per bunch. The above in turn signifies that the limiting collective effects may be of long-range nature lasting longer than the bunch spacing

influencing a train of bunches, or of short-range nature only lasting within a bunch. For a given DLSR, we would therefore have to study the sources driving both short- and long-range collective effects.

The essential feature of the machine optics in reducing the horizontal emittance towards a diffraction limited value is to divide the dipole magnets into a large number of pieces following the well-known dependence of the theoretical minimum emittance (TME) on the third power of the bending angle, and to impose the linear optics to approach the so-called TME condition. The two manipulations above result in suppressing the horizontal dispersion in dipoles to a small value, rendering the momentum compaction factor α, defined by

$$\alpha = \frac{1}{L_c} \oint \frac{D_H}{\rho} ds \tag{1}$$

to become smaller. Here, D_H, ρ and L_c denote respectively, the horizontal dispersion, the effective radius of curvature in a dipole magnet and the machine circumference. The integral over the longitudinal coordinate s is made around the ring. The smaller the momentum compaction α, the larger becomes the isochronicity of the beam, as can be inferred from the bunch length and the synchrotron frequency both scaling with the square root of α. A larger isochronicity tends the beam to be more sensitive to collective instabilities. We shall see in Sec. 4 that several analytical instability threshold formulae do explicitly express such dependence on α. In addition, a shorter bunch tends to be more easily coupled with high frequency wake fields and be more sensitive to micro-bunching (or microwave instability). Imposing the linear optics to approach the TME condition generally requires stronger quadrupole focusing, which results in reducing the bore radius of quadrupoles, and therefore the vacuum chamber aperture, as the vacuum chamber must fit in between the magnet poles. As a consequence, the storage ring shall have limited aperture all around, and since wake fields or the coupling impedance generally scale at least inversely linearly to the vacuum chamber opening, one ends up having large distributed impedance, inevitably enhancing collective effects. On top of which, light source storage rings are made to accommodate a large number of insertion devices, the magnetic gaps of which are generally closed to even smaller values than the distance between magnet poles. Both low gap sections due to resistive-wall, and taper transitions due to geometric impedance, will therefore contribute significantly to the impedance of a DLSR.

The operational aspect of a DLSR, that it must, like all other LSRs (Light Source Rings), deliver synchrotron radiation as constant and stable as possible, has also an indirect link to collective effects.

To achieve the former, the beam lifetime and the injection efficiency must generally be as long and high as possible, which in turn requires the chromaticity to be reasonably small as a large chromaticity tends to limit the dynamic acceptance of a ring. As is known, however, a small value of chromaticity tends to limit the damping of lower-order head-tail modes and thus lower their instability thresholds. Besides, it must also be recalled that the quality of an undulator spectrum depends on the energy spread of a circulating electron beam, the sensitivity of which increases especially for higher-order harmonics. In designing or operating a DLSR, therefore, special care must be taken not to blow up the beam energy spread by the microwave instability.

3. Coupling impedance in DLSRs

As we have seen in the previous section, there are at least two intrinsic reasons for a DLSR to have reduced vacuum chamber apertures distributed all around the ring; one is due to the required stronger focusing of the magnets that tends to reduce the distance between magnetic poles inside of which the vacuum chamber resides, and the other, due to the closing of the insertion device gaps to at least a comparable extent as the existing LSRs. If we plot the vertical half aperture of the standard chamber (chambers in the magnetic sections) b versus the energy E of the machine for a number of existing LSRs along with several DLSRs which are either being built or proposed (Fig. 1), we may confirm the trend as mentioned above. The dashed curve in the figure represents a constant value of $E \cdot b^3$, adjusted to the SOLEIL case, which gives a rough estimate of the impact of resistive-wall instability (cf. Eq. 31 in Subsec. 4.2.1). Whereas, the coupling impedance is a quantity that scales inversely with distance from the beam axis to the chamber walls, as one would intuitively guess. It follows that one should expect an enhanced coupling impedance for a DLSR. Specifically, the dependence is typically inversely linear longitudinally, and inversely quadratic or even cubic transversely as it is for the resistive-wall. Below we shall review the vacuum components contributing to the coupling impedance of a machine along with their general impedance characteristics, by grouping them into geometric and resistive-wall origins. Though in reality, a given vacuum structure normally possesses simultaneously geometric and resistive-wall wakes, we are bound to treat them separately as there is no general method that allows us to solve them together. Since many features are commonly found in existing LSRs, we should stress those that are expected to be particularly important for a DLSR.

3.1. Definition of wake functions and coupling impedance

Before going into the details of the coupling impedance in a DLSR, let us, for the sake of clarity, quickly recall the definitions of the terminologies used, along with their explicit expressions, which can be found in textbooks (Chao, 1993; Zotter & Kheifets, 1998). We shall employ MKSA units.

A longitudinal wake function or a Green's function wake for a given vacuum chamber structure is defined as a voltage seen by a point charge trailing a leading particle having charge q at a distance s

$$W_{//}(s) = \frac{1}{q} \int_{-\infty}^{\infty} E_z(z, \frac{z+s}{c})\, dz \quad \text{[V/C]}, \tag{2}$$

where the integral is performed from minus to plus infinity over the longitudinal coordinate z, $E_z(z, t)$ denotes the longitudinal electric field excited by the leading particle and c the speed of light at which particles are assumed to travel. The sign of s is defined such that the wake function $W_{//}(s)$ is zero for $s < 0$ due to causality. In our convention, a positive wake function signifies that a particle is decelerated. A wake potential is then conventionally given as a convolution of the former with a bunch distribution function $\lambda(s)$ (its integral $\int_{-\infty}^{\infty} \lambda(s')\, ds'$ is normalized to unity)

$$V_{//}(s) = Q \int_{0}^{\infty} W_{//}(s') \cdot \lambda(s - s')\, ds' \quad \text{[V]}, \tag{3}$$

where Q represents the total bunch charge. Instead, one can directly extend the definition of the wake function of a point charge to a bunch wake

$$\mathcal{W}_{//}(s) = \int_{0}^{\infty} W_{//}(s') \cdot \lambda(s - s')\, ds \quad \text{[V/C]}. \tag{4}$$

The longitudinal coupling impedance is defined as a Fourier transform of the wake function

$$Z_{//}(\omega) = \frac{1}{c} \int_{-\infty}^{\infty} W_{//}(s)\, e^{i\omega \cdot s/c}\, ds \quad \text{[}\Omega\text{]}. \tag{5}$$

The loss factor $\kappa_{//}(\sigma)$ of a bunch is given by the integral of its distribution function $\lambda(s)$ with the wake potential $V_{//}(s)$. In the frequency domain, it can be expressed by

$$\kappa_{//}(\sigma) = \frac{1}{\pi}\int_0^\infty d\omega \,\mathrm{Re}\, Z_{//}(\omega)\cdot\left|\tilde{\lambda}(\omega)\right|^2 \quad \text{[V/C]}, \tag{6}$$

where $\tilde{\lambda}(\omega)$ represents the Fourier transform of the distribution function $\lambda(s)$. Now, a transverse wake function or Green's function wake is defined in a similar way as in the longitudinal case, by displacing the leading particle by the amount Δu transversely from the beam axis and normalizing the wake function by it. Namely,

$$W_\perp(s) = \frac{1}{q\,\Delta u}\int_{-\infty}^{\infty} (\vec{E} + \vec{v}\times\vec{B})_\perp \, dz \quad \text{[V/C/m]}, \tag{7}$$

where $\vec{v}$ and $\vec{B}$ represent the leading particle's velocity and the excited magnetic field vectors, respectively. While the transverse wake potential $V_\perp(s)$ is obtained from the convolution of the transverse wake function with the distribution function $\lambda(s)$, as in Eq. 3, the transverse coupling impedance $Z_\perp(\omega)$ is conventionally defined as a Fourier transform of $-i\cdot W_\perp(s)$,

$$Z_\perp(\omega) = -\frac{i}{c}\int_{-\infty}^{\infty} W_\perp(s)\, e^{i\omega\cdot s/c}\, ds \quad \text{[}\Omega\text{/m]}. \tag{8}$$

The counter part of the loss factor in the transverse plane is the kick factor $\kappa_\perp(\sigma)$, which can be expressed in the frequency domain as

$$\kappa_\perp(\sigma) = -\frac{1}{\pi}\int_0^\infty d\omega \;\mathrm{Im}\, Z_\perp(\omega)\cdot\left|\tilde{\lambda}(\omega)\right|^2 \quad \text{[V/C/m]}. \tag{9}$$

3.2. Geometric impedance

The overall characteristics of the geometric impedance of a DLSR are expected to remain similar to those of the existing 3rd generation LSRs as the constituent vacuum components are likely to be analogous, although in magnitude, they may generate a larger impedance due to the reduced chamber aperture as mentioned above. The total impedance of a ring is usually determined by vacuum components that exist in numbers even if each individual contribution is not necessarily large, and by those whose single component impedance is large. The vacuum elements that usually represent the

former are shielded bellows, flanges and BPMs, pumping holes and ante-chamber slots, while cavities, tapers, scrapers, striplines and kickers belong to the latter group.

Let us begin with the first group of objects. Vacuum pumping holes and shielding RF fingers are generally found through numerical studies to contribute little to the impedance from their optimized geometric shapes. On the other hand, a small taper with a tiny step of typically a fraction of a milimeter often emerging from two RF finger foils sliding one on top of the other, may produce a non-negligible impedance contribution. In addition, a thin longitudinal slit between two plates of a flange can generates a series of high Q resonances that can be a dangerous source of trapped modes. In fact, the SOLEIL flange, having a slit of 0.4 mm longitudinally and 50 mm radially, turned out to create trapped modes, strong enough to induce coupled-bunch instabilities with unacceptably low thresholds. As a remedy, a metallic foil was introduced to shield the small cavity structure exposed to the beam, which successfully eliminated the excitation of the trapped modes (Fig. 2) (Nagaoka, 2004). In this respect, the new flange design of Sirius (Fig. 3), adopting the idea of KEK (Matsumoto *et al*., 2006) that completely eliminates the slit by means of a gasket inserted between the two plates, is optimal from the impedance point of view and may be a promising solution for future DLSRs (Seraphim, 2014).

A small gap between an electrode and its surrounding block, such as in a BPM, also represents a dangerous source of impedance and trapped modes. Here, one obviously cannot adopt the recipe of short-circuiting the gap as was done above for a flange. One would need to study the way the trapped modes depend on the geometry of the electrode such as its thickness or surface area in conjunction with the overlap of the bunch spectrum in order to decouple the beam from the impedance. For a BPM, reducing the button radius has the beneficial effect of increasing the trapped mode frequency away from the beam, which however reduces the button sensitivity that scales as the square of the button radius. For a DSLR that requires excellent BPM reading accuracy, therefore, other means need be explored. In the case of a SOLEIL BPM, the button thickness was increased from its original value of 2 mm to 5 instead of reducing the button radius, which managed to reduce the loss factor by as much as a factor of two. A larger thickness button is considered to help filter out high frequency trapped modes in the gap via its increased capacitance (Nagaoka *et al.*, 2006). Interesting studies are underway at Sirius optimising the button shape, such as a bell-shape, (Fig. 4) so to increase the trapped mode frequency without losing the button sensitivity (Caiafa, 2014). Slots between chambers and ante-chambers or for the extraction of synchrotron radiation have not been reported to cause significant problems of impedance up to now, apart from some limited cases in which trapped modes apparently disturbed the BPM reading. The small slot impedance found in the existing LSRs should be thanks to the use of flat chambers that allowed the slots to be positioned relatively far from the beam horizontally. If circular chambers are to be adopted for a DLSR, as in the case of MAX IV (Al-

Dmour, 2011) and Sirius (Sirius, 2013), the impact of the slot impedance would have to be re-investigated.

Now looking into the second group, taper transitions are still expected be those that make the largest contributions to the impedance budget for a DLSR, and would require special efforts to minimize. With a reduced chamber aperture in the magnet sections, one might think that the smaller relative difference to low insertion device gaps would lower the taper impedance. This would however not be entirely true since even though the taper angle may get smaller for the same taper length, the distance from the beam axis to where taper exists also plays a role, as was already argued previously. The latter aspect is particularly true transversely, as can be seen in the taper impedance formula derived by K. Yokoya for a cylindrical taper (Yokoya, 1990),

$$Z_{\perp}(\omega) = -\frac{iZ_0}{2\pi}\int_{-\infty}^{\infty} \frac{1}{b(z)^2}\left(\frac{db(z)}{dz}\right)^2 dz\,, \tag{10}$$

where $b(z)$ denotes the chamber radius as a function of the longitudinal coordinate z, and Z_0 is the vacuum impedance. Tapers are known to be inductive as above in the low frequency regime and can exhibit resonant behaviour at high frequencies involving resistive components. As spatial constraints are expected to become even more stringent for a DLSR, minimization of the taper impedance for a given length would continue to be an important issue. In view of the radial dependence of the taper impedance as in Eq. 10, attempts are made to minimize the slope where the aperture is small and increase it where the aperture is larger, namely a nonlinear taper, so as to minimize the total taper impedance (Podobedov, 2007) For variable tapers such as those for in-vacuum insertion devices, it is important that the taper geometry is optimized for all gaps. The same argument clearly holds for variable scrapers as well. At SOLEIL serious problems of beam-induced heating occurred when the gap was set at the standby or the fully open position, which turned out to be due to the appearance of a cavity-like structure in that position, while the taper geometry was optimized for the minimum gap position (Nagaoka, 2007).

RF cavities are expected to remain being the major impedance contributors in the impedance budget due to their geometries. It is important to fully characterize their impedance quantitatively including HOMs. Their relative contributions would increase for DLSRs that plan to install bunch lengthening harmonic cavities, which are becoming an important option in stabilizing the beam against collective effects (see Subsec. 7.3 for more details). Striplines are expected to be indispensable devices in a DLSR for transverse bunch by bunch feedback, and possibly for on-axis bunch by bunch

injection as well, as being considered at APS (Xiao, 2013). An innovative design developed at SOLEIL, embedding the electrodes in the vacuum chamber such that they match the chamber inner surface (Fig. 5), allowed creating a highly efficient stripline simultaneously having impedance merely comparable to a single BPM (Mariette *et al*., 2007). Continuous efforts in this direction appear worthwhile.

Although there are a number of analytical models describing the impedance of the objects discussed above (e.g. Zotter & Kheifets, 1998; Ng & Bane, 2010), they are generally limited to structures having cylindrical symmetry and are also limited to low frequencies, which signifies the complexity of the subject. Though there exist a few marked studies in this direction (Bane, Stupakov, Zagorodnov, 2007; Stupakov, Bane, Zagorodnov, 2007), a more general and reliable method, applicable in principle to any 3D structure, would therefore be the numerical solution of the Maxwell equations using the codes developed for this purpose, such as *ECHO* (Zagorodnov & Weiland, 2005), *GdfidL* (Bruns, 1996) and *CST microwave-studio* (CST Microwave Studio, 2014). The numerical computations, however, also have their known limitations due to vacuum chamber dimensions in relation to the concerned bunch length. Often computations become infeasible either memory-wise or computation-time-wise. In many chamber structures, computations are bound to be three-dimensional, due to a non-circular chamber cross section, or to non-uniformity of the structure azimuthally. The shortness of the bunch length in a DLSR, as well as the fineness of structure features, such as the gap between a BPM button and its surrounding block tends to require meshing of the computational volume to a dimension smaller than a fraction of a milimeter. Following the excited wakes in time, which is particularly important for long surviving wakes such as trapped modes, is another area that requires special effort of intensive computations. As already stated, a detailed examination of trapped modes for a given vacuum component would be particularly important for a DLSR, due to its reduced chamber aperture and shorter bunch nature. The numerical solution of Maxwell's equations in the time domain is also known to be susceptible to certain errors such as mesh dispersions. Benchmarking of different codes available therefore is important in understanding the limits of each code as well as its characteristics, in comparison with others. Several studies are being made in this direction (Blednykh, 2014; Caiafa, 2014).

Generally, the purpose of impedance calculations for a DLSR would at least be twofold: to evaluate and minimize the impedance of individual vacuum components, and to use the obtained total impedance for beam instability studies. The latter motivates one to compute wake potentials for a short bunch, and in fact for the shortest possible bunch, since what we need in instability simulations are Green's function wakes that we can convolute with arbitrary bunch distributions. In addition to simply identifying the wake potentials obtained in this way as "pseudo Green's functions", efforts have been made to deduce causal wake functions from the former. Driven by the needs to explore wakes excited by extremely short bunches produced in modern linear accelerators, analytical studies

were made to pursue very short range wakes or very high frequency impedances, where it was found that many short range wakes reduce to what can be described by relatively simple models such as diffraction and optical models (Bane & Sand, 1987; Bane, Stupakov, Zagorodnov, 2007). Extending the studies further along this line, there have recently been attempts to combine the former analytical models with numerical solutions to obtain wakes excited by a point charge in a general structure (Podobedov & Stupakov, 2013). Such approaches may yield breakthroughs to numerical limitations in the studies of collective effects in a DLSR.

Before closing this section, let us look at two examples of impedance budgets calculated for DLSRs, one for MAX IV (Klein *et al*., 2013) and the other, for PEP-X (Bane, 2013). For MAX IV, the sums of impedance are plotted in different colours to distinguish the different contributions, respectively in the longitudinal, horizontal and vertical planes (Figs. 6). In the longitudinal plane, the impedance divided by n ($\equiv \omega/\omega_0$, ω_0: angular revolution frequency) is plotted to render the numerical comparison with other machines simpler. Reflecting on the fact that most vacuum elements are inductive at low frequencies and become resistive at high frequencies, the overall impedance is indeed found to be inductive at low frequencies with broad resonance-like structures at high frequencies. It should be noted that the ensemble of BPMs and bellows makes a large contribution. The computation does not yet include insertion device tapers, as they have not yet been fully defined; however, they are expected to contribute significantly in the budget. Another point to be noted is the difference in the impedance distributions in the two transverse planes (the central and right columns in Figs. 6), even though the evaluated chambers are all circular. Being transverse, weighting of the transverse impedance by the beta functions was made to take into account the important optics dependence, normalized by the average beta values. Transverse beam instabilities are expected to differ between the two planes reflecting this difference, which is an important aspect in the impedance optimisation and analysis.

Table 1
Impedance budget for PEP-X, giving the loss factor, effective resistance and inductance of various objects in the ring. The results are obtained at nominal bunch length σ_z = 3 mm (Bane, 2013)

Object	Single Contribution			Total contribution			
	k_{loss}[V/pC]	R [Ω]	L [nH]	N_{obj}	k_{loss}[V/pC]	R [Ω]	L [nH]
RF cavity	0.92	30.4	-	16	14.7	487	-
Undulator taper (pair)	0.06	3.2	0.32	30	1.9	95	9.6
Wiggler taper (pair)	0.43	21.4	0.72	16	6.8	340	11.5
BPMs	0.013	0.6	0.005	839	11.3	465	4.1
Bellows slots	0.00	0.0	4e-4	720	0.0	0.0	0.3
Bellows masks	0.005	0.2	0.004	720	3.7	142	2.7
Resistive-wall wake					21.3	880	11.3
Total					59.7	2409	39.5

Table 1 summarizes the longitudinal impedance budget estimated for PEP-X for a nominal bunch length of 3 mm. It can be seen that the BPMs as a whole make a large contribution to the loss factor even though individually, they are small. Insertion device tapers are seen to make a significant contribution to the loss factor as well. Reflecting the importance of low gap sections, the resistive-wall makes the major contribution (~30%) to the loss factor.

3.3. Resistive-wall and dielectric material wall impedance

The fact that a DLSR would inevitably choose to install vacuum chambers having smaller aperture as compared to the existing LSRs raises, above all, the problem of the resistive-wall impedance, as we may recall that the transverse resistive-wall impedance scales as the cube of the half aperture b(s). The restive-wall impedance per unit length of a circular chamber of radius b is familiarly given in the longitudinal and transverse planes by

$$\frac{Z_{//}^{RW}(\omega)}{L} = \frac{e^{-i\pi/4}}{2\pi}\cdot\frac{1}{b}\sqrt{\frac{Z_0\rho_r\omega}{c}} \quad [\Omega/\mathrm{m}], \tag{11}$$

and

$$\frac{Z_{\perp}^{RW}(\omega)}{L} = \frac{e^{-i\pi/4}}{2\pi}\cdot\frac{2}{b^3}\sqrt{\frac{cZ_0\rho_r}{\omega}} \quad [\Omega/\mathrm{m}^2], \tag{12}$$

respectively. Here, ρ_r is the resistivity of the chamber material. As is well-known, the resistive-wall impedance has both narrow and wide band feature, which is equivalently long and short range fields in time domain, thus being capable of inducing both multi and single bunch instabilities. In particular, its narrow-band with its increasing amplitude towards zero frequency shall be the strong source of resistive-wall instabilities in a DLSR (see Sec. 4.2.1). On the other hand, as the longitudinal resistive-wall impedance depends merely inversely linearly on b(s), there should be no significant increase of its contribution in a DLSR as compared to the existing LSRs.

As already stated, the evaluation of the resistive-wall impedance is normally done separately from those of the geometric impedance since the numerical treatment of the skin depth effect is generally

difficult, due both to the thinness of the skin depth and to the much longer time scale involved. Fortunately, resistive-wall wakes and impedance can be analytically calculated in many cases of interest. The formulae in Eqs. 11 and 12 are the most familiar ones deduced for a circular cross section chamber with infinitely thick resistive-wall. Deviations from this simple case were studied in many directions; short-range wakes correcting the fictitious divergence of the thick wall wakes (the Fourier transforms of Eqs.11 and 12) occurring at the origin on the time axis (Henry & Napoly, 1991; Bane & Sands, 1995), wakes for finite thickness walls (Zotter, 1969), as well as for non-circular chamber cross sections (Gluckstern *et al*., 1992; Yokoya, 1993). Wakes for multi-layered resistive-wall chambers (Chao, 1993; Zotter & Kheifets, 1998; Burov & Lebedev, 2002). With its enhanced sensitivity to resistive-walls, all these specific features would be important for a DLSR to take the resistive-wall effect correctly into account quantitatively.

Of particular relevance would be the multi-layered resistive-wall models, since metallic coatings such as copper coating for improved electric conductance and NEG coating for distributed pumping, have already been the well-established techniques in many existing light sources. With the anticipated reduced vacuum conductance due to smaller aperture, the latter would be of increasing importance for a DLSR. There are concerns, however, that NEG coating enhances the impedance of a machine, which follows the observations made at Elettra (Karantzoulis *et al*., 2003). Namely, it was observed in a reproducible manner that the increment in the slope of the single bunch vertical coherent detuning was effectively double for a NEG coated chamber as compared to the same chamber without NEG coating. Employing a multi-layer resistive-wall formula, it was found that, the model qualitatively explains the increase of the reactive part of the impedance with NEG coating. However, quantitatively the increment was too small to explain the measurement. To match the observation, one had to assume unreasonably large values of both the resistivity of NEG and the coating thickness (Nagaoka, 2004). The possibility of roughness impedance was then argued as a result of eventual poor coating quality.

Impedance studies of ceramic chambers used for pulsed magnets should also be of increasing importance for a DLSR, always in view of the reduced distance from the beam to the chamber wall. To allow the image current to flow on the wall surface, a metallic coating, such as of titanium, must be introduced, for which the coating thickness must however be carefully studied to make the best compromise between the magnet performance and the beam-induced heating. There again, the impedance of a multi-layer object, now including dielectric materials must firstly be worked out, such as the one derived by Nagaoka *et al*., (2006). The longitudinal impedance per unit length reads,

$$\frac{Z_{//}(\omega)}{L} = \frac{-i}{2\pi\varepsilon_0 cb}\left\{\left(\frac{a}{k}-\frac{k}{a}\right)\cdot\frac{\left[1+A\tanh(ad)\right]}{\left[A+\tanh(ad)\right]}-\frac{kb}{2}\right\}^{-1} \quad [\Omega/\mathrm{m}], \tag{13}$$

where $k = \omega/c$, $a = [1\text{-}i\cdot\mathrm{sgn}(\omega)]/d_s$ (d_s: skin depth), d the metallic (titanium) coating thickness, A is equal to $A_0 \equiv i(a/k - k/a)\sqrt{\mu_r\varepsilon_r - 1}/\varepsilon_r$ for infinitely thick ceramic, or to $-iA_0\tan(\nu d_c)$ when the thickness is d_c, with $\nu = k\sqrt{\mu_r\varepsilon_r - 1}$. Other symbols have their usual meanings. The beam induced power P_s can be calculated from the above formula for a given beam current and coating thickness following the relation given in Eq. 6. Now in case the chamber is non-circular and elliptical, as in the current design of a multipole injection kicker for MAXIV (Lebasque, 2013), the surface power density must be calculated in order to estimate the temperature rise, as the power would be sharply concentrated on the upper and lower surfaces closest to the beam. Following the work of Piwinski (1992) on a flat chamber, its distribution as a function of the horizontal displacement x can, to a good approximation, be given by (Nagaoka *et al.*, 2006)

$$P_s(x) = \frac{\pi^2}{4\cosh^2(\frac{\pi}{2b}x)} \cdot (P_s)_{circle} \tag{14}$$

where $(P_s)_{circle}$ denotes the surface power density of a circular chamber of radius b.

3.4. Coherent Synchrotron Radiation (CSR) wakes and impedance

A short, relativistic bunch moving in a circle in free space will radiate coherently at wavelengths that are long compared to the bunch length; this radiation is called coherent synchrotron radiation (CSR). In a storage ring CSR can induce longitudinal microwave instability. However, in a ring, unless the bunch is very short, the vacuum chamber walls will shield and suppress the CSR, which is the main reason why the CSR instability is not observed in most storage rings. However, there are light sources, such as Metrology Light Source (MLS) and BESSY-II, which operate at least part of the time in low α mode to shorten the bunch, and then provide the induced CSR radiation to their users. For DLSRs such instability is something normally to be avoided.

The CSR impedance including shielding has been studied already since many years, beginning with Schwinger (1945), and including also Nodvick & Saxon (1954), and Faltens & Laslett (1973). With the recent interest in short bunches a compact form of the free-space CSR wake was developed by Derbenev *et al.* (1995), and then the short-range wake for a bunch moving between two parallel conducting plates by Murphy *et al.* (1997).

3.4.1. CSR wakes

Assume that two relativistic particles in free space follow each other on a circle of radius ρ. The longitudinal wake, with test particle at position s behind the driving charge, can be approximated (Derbenev, 1995, Murphy *et al.*, 1997)

$$\frac{W_0(s)}{L} = -\frac{Z_0 c}{2\pi} \cdot \frac{H(-s)}{3^{4/3}\rho^{2/3}(-s)^{4/3}}, \tag{15}$$

with $H(s) = 1$ (0) for $s > 0$ ($s < 0$). Note that, unlike for the other wakes, in the case of free-space CSR, the driving particle needs to be behind the test particle for the wake to be non-zero, and that the overall minus sign indicates energy gain by the test particle. The formula is a "long-range" approximation, valid for $(-s) >> \rho/\gamma^3$, where γ is the Lorentz factor; at very short distances the wake changes sign so that the test particle loses energy; at the origin, the wake $W_0(0-) \sim \gamma^4/\rho^2$. For smooth bunch shapes of rms length $\sigma_z >> \rho/\gamma^3$, one needs not know the details of the wake near the origin; the bunch wake is simply given from the asymptote $W_0(s)$ by

$$W_\lambda(s) = -\int_{-\infty}^{0} W(s')\,\lambda(s-s')\,ds' \approx -\int_{-\infty}^{0} S_0(s')\,\lambda'(s-s')\,ds', \tag{16}$$

with $W(s)$ the actual point charge wake, the one that is valid all the way down to $s = 0$; $\lambda'(s)$ is the derivative of the bunch distribution, and $S_0(s) = \int_{-\infty}^{-s} W_0(s')ds'$. This trick for obtaining the bunch wake from an asymptotic wake function of the form $W_0(s) \sim s^{-1-\alpha}$ with $0 < \alpha < 1$, has long been used with e.g. the longitudinal resistive wall wake field. The free space CSR bunch wake for a Gaussian distribution is given in Fig. 7.

It has long been known that a vacuum chamber can suppress the CSR wake, if the bunch length $\sigma_z \gtrsim a^{3/2}/\rho^{1/2}$, where here a represents either the radius of a round pipe or the half-height of a flat one (see e.g. Warnock, 1990). Murphy *et al.* (1997) found the short-range wake of a particle moving in a circle in the midplane between two perfectly conducting, parallel plates. For this case the total point

charge wake can be written as $W_{tot}(q) = W_0(q) + W_1(q)$, with $q = s/\sigma_{z0}$. If the plates are located above and below the beam orbit, at $y = \pm h$, then (Murphy *et al.*, 1997, Bane *et al*., 2010)

$$\frac{W_1(s)}{L} = -\frac{Z_0 c}{8\pi^2 \rho^{2/3}} \left(\frac{\Pi}{\sigma_{z0}}\right)^{4/3} G\left(\frac{\Pi s}{\sigma_{z0}}\right), \tag{17}$$

with shielding parameter $\Pi = \sigma_{z0}\rho^{1/2}/h^{3/2}$. The function $G(\zeta)$ is expressed as a sum that typically is well converged at 25 terms. $W_1(s)$ is part of a point charge wake, and in principle any scale factor, σ_{z0}, can be used here. Note that the function $W_1(s)$ --- unlike $W_0(s)$ --- in general, is non-zero for all s. To demonstrate the effect of shielding, we give in Fig. 8 the ratio of the loss factors for the shielded and unshielded cases, $f_{sh} = \kappa_{sh}/\kappa_{free}$, as function of Π. We see that the loss factor drops exponentially with Π; the dashed curve in the figure gives the Gaussian fit $e^{-(\Pi/\sigma)^2/2}$, with $\sigma = .609$.

3.4.2. CSR impedance

For the case of an ultra-relativistic beam moving in a circle of radius ρ in free space:

$$\frac{Z(\omega)}{L} = \frac{Z_0}{2\pi} \frac{\Gamma(2/3)}{3^{1/3}} e^{\pi i/6} \left(\frac{\omega}{c\rho^2}\right)^{1/3}, \tag{18}$$

with the Gamma function, $\Gamma(2/3) = 1.354$. The shielded model impedance has been studied and understood almost as long. In longitudinal instability analysis in rings it is $Z(n)/n$ that is important, with $n = \omega/\omega_0 = \omega\rho/c$ (ω_0 is the revolution frequency). For example, it has been known that, for the shielded model, there is a broad peak in $Re(Z)$ at $\omega \approx c\rho^{1/2}/h^{3/2}$ with a peak value $Re(Z(n))/n \approx (300\ \Omega)(h/\rho)$ (see e.g. Lee *et al*., 1983). In a recent paper Y. Cai (2011) gave a formulation of this model in terms of scaled parameters. In Fig. 9 we present his plot that shows $Z(n)/n$, with Z the impedance per turn, for both shielded and unshielded models. At high frequencies the two models yield the same values (shielding has no effect). We see that shielding effectively suppresses $Re(Z)$ for frequencies $(\omega h^{3/2}/c\rho^{1/2}) \lesssim 0.6$. It is interesting to note that there is an extended frequency range where the real part of the impedance $Re(Z)$ is larger for the shielded than for the unshielded model.

Real vacuum chambers are generally closed chambers. Warnock & Morton (1990) found the impedance of a torus with a rectangular cross-section by field matching, in terms of high order Bessel

functions. They found whispering gallery-like modes giving a forest of high frequency spikes in $Re(Z(\omega))$. Unlike for an open structure like the parallel plates, the closed toroid has resonances. This means that in addition to a short-range wake, the closed toroid CSR wakes can in principle generate significant bunch-to-bunch interactions. An example calculation for the ANKA ring, showing $Re(Z)$ in [Ω] as function of $(\omega/2\pi c)$ in [cm^{-1}], is given in Fig. 10 (Warnock *et al*., 2013). The circumference of ANKA is 100 m, ρ = 5.6 m, height of the chamber h = 1.6 cm, and its width ω = 6.8 cm. We see that $Re(Z)$ peaks at $\lambda^{-1} \approx 5$ cm^{-1}, or $n \approx 20{,}000$, with a maximum value of 400 kΩ.

In a ring, the formula for obtaining the bunch wake from the impedance,

$$W_\lambda(s) = -\frac{c}{2\pi}\int_{-\infty}^{\infty} Z(\omega)\cdot\tilde{\lambda}(\omega)\, e^{-i\omega s/c} d\omega\,, \tag{19}$$

becomes (Venturini & Warnock, 2002)

$$W_\lambda(s) = -\frac{c\omega_0}{2\pi}\sum_n Z(n)\,\lambda_n\, e^{-ins/\rho} \tag{20}$$

with

$$\lambda_n = \frac{1}{c}\int_0^{2\pi\rho} \lambda(s)\, e^{ins/\rho} ds\,. \tag{21}$$

The calculation of the CSR wake/impedance and its effect has recently become a very active field of study. For example, Stupakov & Kotelnikov (2003, 2009), through field matching, have found the CSR impedance for circular chambers and for the case of a bend chamber followed by a straight pipe; they found, in particular, that the paraxial approximation to the wave equation can be applied, allowing for mesh-based calculations of modes with mesh sizes much larger than the wavelengths of interest. Building on this work, algorithms have been developed for chambers with a rectangular cross-section, and with the beam passing through bend and drifts by Agoh & Yokoya (2004), and

Zhou (2011). In principle, the CSR wake of a vacuum chamber with arbitrary cross-section, with the beam passing through bends and drifts representing an entire ring, can now be modeled.

Normally, however, the vacuum chamber cross-section is different in different parts of a ring, with transitions connecting the different parts. CSR simulations of ring vacuum chambers including such transitions are still beyond the current state of the art. Nevertheless, simple models like the parallel plates and the rectangular chamber have, at times, been shown to work extremely well when used in simulations and then compared with measurements; see e.g. for the Metrology Light Source (MLS; for threshold to instability (Ries *et al*., 2012)) and the National Synchrotron Light Source's (NSLS) UV ring (for bursting mode spectrum (Zhou, 2011)).

4. Beam instabilities in DLSRs

As described in the previous sections, the fact of having reduced vacuum chamber aperture distributed around a DLSR enhances both the geometric impedance that generally has short temporal range and the resistive-wall impedance which, on the contrary, is known for its long-range nature. While the former predominantly influences collective motions of a single bunch, the latter, of multiple bunches. Below we shall treat them separately and review those that are considered to be particularly dangerous for a DLSR. It must be noted that the enhanced sensitivity of a DLSR against collective effects may even be such that, single bunch instabilities become a concern for a machine running exclusively in a multibunch mode, due to their thresholds getting as low as the bunch current in the respective mode.

4.1. Single bunch instabilities

4.1.1. Bunch lengthening

As in the existing LSRs, a bunch in a DLSR would initially evolve in the PWD (Potential Well Distortion) regime when its current is raised from zero due to the usually inductive nature of the machine impedance, which can be described by the following relation deduced from the Haissinski equation (Chao, 1993; Limbourg, 1996)

$$\left(\frac{\sigma_l}{\sigma_{l0}}\right)^3 - \left(\frac{\sigma_l}{\sigma_{l0}}\right) = \frac{1}{4\sqrt{\pi}} \cdot \frac{-2\pi i I \left|\frac{Z_{//}(\omega)}{n}\right|_{eff}}{V_{rf} h \cos\varphi_s \left(\frac{\omega_0 \alpha}{\omega_{s0}} \sigma_\varepsilon\right)^3}. \qquad (22)$$

It can be seen that, both, a likely enhancement of the machine impedance and a smaller momentum compaction α, along with a smaller energy spread σ_ε in a DLSR tend to enhance the bunch lengthening. Not only would vacuum components listed earlier such as tapers, BPMs, and shielded bellows contribute to the inductive impedance, but a reduced aperture around the machine would also increase the relative contribution of the resistive-wall, which is inductive as well. For a Gaussian bunch, the effective longitudinal resistive-wall impedance seen by the beam can be evaluated by

$$\left|\frac{Z_{//}^{RW}(\omega)}{n}\right|_{eff} = \frac{\Gamma(1/4)}{b}\sqrt{\frac{\sigma_l Z_0 \rho_r}{2\pi}} \qquad [\Omega] \tag{23}$$

where $\Gamma(1/4) = 3.6256$. In the impedance budget of MAXIV referred to earlier, the effective resistive-wall impedance amounts to ~90 mΩ from the expression above assuming the resistivity of copper (1.7×10^{-8} Ω·m). With 390 mΩ coming from the geometric impedance, it roughly represents 20% of the total impedance. We note that if instead the resistivity of the order of 100×10^{-8} Ω·m is employed in the above equation, which is not impossible as that of NEG used for coating, the resistive-wall contribution exceeds that of the geometric impedance. The bunch lengthening in the PWD regime is known to associate no energy spread widening. For a DLSR, the enhanced bunch lengthening would therefore be favored in most cases, as it helps fight against IBS and reduced Touschek lifetime, which are the serious issues in a DLSR (cf. Sec. 5). In fact, many DLSRs may decide to lengthen bunches with harmonic cavities (cf. Subsec. 7.3). For completeness, the expression corresponding to Eq. 23 for the transverse resistive-wall impedance reads

$$\left|\frac{Z_{\perp}^{RW}(\omega)}{L}\right|_{eff} = \frac{\Gamma(1/4)}{\pi b^3}\sqrt{\frac{\sigma_l Z_0 \rho_r}{2\pi}} \qquad [\Omega/\mathrm{m}^2]. \tag{24}$$

4.1.2. Microwave instability

As contrary to the bunch lengthening above, the microwave instability should be totally avoided in many DLSRs as it involves energy spread widening. The latter deteriorates higher-harmonic undulator spectra, the use of which is critically important for low and intermediate energy DLSRs. Whereas, for high energy DLSRs, both the energy spread widening as well as the anomalous bunch lengthening in the turbulent regime may be beneficial for mitigating IBS and Touschek scattering, especially in view of no risk of losing the beam from this instability. Unlike the previous bunch lengthening in the PWD regime, the microwave instability involves coupling of the beam with the resistive impedance,

inducing micro-bunching or turbulent motions of the beam. It has been studied since long in proton storage rings for high energy physics prior to the appearance of LSRs. The instability threshold derived in the coasting beam theory is known as Keil-Schnell criterion (Keil & Schnell, 1969), which was later extended by D. Boussard to a bunched beam, who judiciously replaced the beam current in the formula by the peak current. The Boussard's criterion then reads (Boussard, 1975)

$$\frac{e\hat{I}\,|\,Z_{//}(\omega)/n\,|}{2\pi\alpha E\sigma_{\varepsilon}^{2}} \leq 1, \tag{25}$$

where $\hat{I}$ is the peak current given by

$$\hat{I} = \frac{\sqrt{2\pi}I}{\omega_0\sigma_l/c} \tag{26}$$

and E denotes the beam energy, c the speed of light and ω_0 is the angular revolution frequency. It was however argued that extrapolation of coasting beam theory to bunch beam exhibits ambiguity especially in the use of the effective impedance in the threshold formula, introducing significant discrepancies to experimental results (Limbourg, 1996). Oide and Yokoya (1990) developed a bunched-beam formalism and pointed out the importance of using a bunch distribution distorted in the PWD, which much improved the former that often gives a large underestimation of the threshold current. Today, multi-particle tracking using realistic impedance is considered to be one of the best methods of simulating the microwave instability. A result of such study made for MAXIV is shown in Fig. 11, where the energy spread of a single bunch is followed versus bunch current using the code *mbtrack* with numerically obtained wake functions (Klein *et al*., 2013). In the figure, the bunch current is indicated on the upper horizontal axis. In the tracking, the bunch current is increased at every 10000 turns by 0.5 mA at moments as indicated by the markers (stars and rectangles). The gray horizontal line in the figure indicates the natural energy spread value of 7.69×10^{-4}. It is found that the energy spread remains constant over the designed operating range, though the microwave threshold is not far above the foreseen maximum single bunch current stored. The bunch lengthening with harmonic cavities is expected to further raise the microwave instability threshold.

It should be noted that the microwave instability due to the CSR wake is currently a topic of much interest and study, both theoretically and experimentally. As a theoretical example, in Bane, Cai & Stupakov (2010), for the shielded CSR model of Sec. 3.4, the threshold current was calculated as

function of shielding parameter, using a Vlasov-Fokker-Planck (VFP) solver (Warnock & Ellison, 2000) and also checked using a linearized Vlasov (LV) solver. The results of the instability study are summarized in Fig. 12. Shown is the normalized strength parameter $S_{csr} = I\rho^{1/3}/\sigma_{z0}^{4/3}$ at threshold [$(S_{csr})_{th}$] *vs.* shielding parameter $\Pi = \rho^{1/2}\sigma_{z0}/h^{3/2}$. Here the normalized current $I = r_e N_e/(2\pi\nu_s\gamma\sigma_{\delta 0})$, with r_e = 2.82 $\times 10^{-15}$ m the classical radius of the electron; with N_e the population, ν_s the synchrotron tune, γ the energy factor, and $\sigma_{\delta 0}$ the nominal (relative) rms energy spread of the bunch. Other parameters are the bending radius ρ, the nominal rms bunch length σ_{z0}, and the half-gap of the shielding plates h. We see that, except for a dip near $\Pi = 0.7$, the numerical results closely follow the straight line $(S_{csr})_{th} = 0.5 + 0.12\Pi$ (the dashes in the plot).

4.1.3. TMCI and head-tail instabilities

Both TMCI (Transverse Mode Coupling Instability) and head-tail instabilities are transverse single bunch instabilities that are considered to be dangerous and potentially performance limiting instabilities for DLSRs. The reasons are that, as already mentioned earlier (cf. Sec. 2), the short-range wake gets stronger due to the reduced chamber aperture, a bunch tends to be shorter (as long as it is not lengthened explicitly), as well as that the momentum compaction factor becomes lower, all of which raising the beam sensitivity to the above instabilities. As being the transverse instabilities, injection saturation or beam losses occur when thresholds are hit. They are harmful in many existing LSRs and show up predominantly in the vertical plane as the vacuum chamber aperture is normally much more reduced in the respective plane. The above signifies that if circular chambers are to be adopted for a DLSR, they could appear equally in the horizontal plane as well. A special effort must therefore be made to study them in advance and take preventive measures.

Strictly, TMCI occurs at zero chromaticity. The most likely scenario for a DLSR is that the lowest head-tail mode 0 is detuned downwards with beam current by the inductive impedance until it couples with its neighboring mode -1, which is roughly one synchrotron frequency away and staying around its original mode frequency. The mode 0 detuning can be described by

$$\frac{df_\beta}{dI} = -\frac{c\beta_0}{8\pi^{3/2}\sigma_l E/e}\cdot \mathrm{Im}\left(Z_\perp\right)_{eff} \quad \text{[Hz/A]}, \tag{27}$$

where f_β is the mode 0 frequency and β_0 is the average beta function value at the impedance locations in the concerned plane. The above expression can be derived from the formalism developed by Satoh and Chin (1983). As seen in the above equation, the slope of the detuning is inversely proportional to

the bunch length. The presence of resistive impedance gives the coupling between the two modes when they meet each other and hence determines the growth rate of the instability. Deriving the TMCI threshold as the current that corresponds to when the mode 0 detuning equals the (incoherent) synchrotron frequency f_s,

$$\left(I_{th}\right)_{TMCI} = \frac{4\alpha\gamma E/e}{\beta_0}\sqrt{\frac{\pi C_q}{J_\varepsilon \rho}}\frac{1}{\mathrm{Im}(Z_\perp)_{eff}}, \tag{28}$$

where α and γ are respectively the momentum compaction and the relativistic energy factors, C_q = 3.84×10^{-13} [m], and J_ε is the longitudinal damping partition number. It is worth noting that, unlike the mode 0 detuning in Eq. 27, the TMCI threshold above does not explicitly depend on the bunch length, as the dependence is canceled out between the slope and the synchrotron frequency.

To avoid TMCI, the chromaticity is conventionally shifted to a positive value, which damps the mode 0. However, a positive chromaticity often renders certain higher-order head-tail modes unstable. Since the latter type of instabilities normally does not involve mode coupling, their thresholds are determined by the sources of damping in the machine, above all, by the radiation damping. The first unstable mode is usually mode -1 and it may happen that its threshold current is even lower than that of TMCI, as observed in several existing LSRs (Revol *et al*., 2000; Harkay *et al*., 2002). If instead, the threshold is sufficiently high as it is often the case for modes superior than -1, the bunch lengthening with current helps pushing the threshold further above. In this way, we can pursue a current threshold curve as a function of the chromaticity. At low positive chromaticities, the threshold is defined by a series of higher-order head-tail modes that successively become unstable one after another, while at higher chromaticity, several modes may simultaneously become unstable creating much more complicated dynamics. Such regime was theoretically and experimentally studied at the ESRF, where it was named post-head-tail instability (Kernel, P. *et al*., 2000).

TMCI and head-tail instabilities can be analyzed in the frequency domain by solving a linearized Vlasov equation decomposed into azimuthal and radial modes. A code such as MOSES numerically solves the equation to obtain complex coherent frequency of modes, with which instability thresholds can be estimated (Chin, 1988). However, for a DLSR in which bunch lengthening and synchrotron tune spreads are likely to give significant effects, 4D (or 6D) multi-particle tracking using realistic (numerically obtained) impedance models would give a more quantitatively satisfying estimate of the instabilities. As in the previous subsection, an example is shown in Fig. 13, where vertical single bunch threshold currents computed by *mbtrack* are plotted as a function of chromaticity for MAXIV, under several different conditions (Klein *et al*., 2014). It is interesting and important to see that the

longitudinal collective effects and harmonic cavity lengthening both help additively to increase the threshold currents, except at zero chromaticity for TMCI, in agreement with the argument above regarding Eq. 28. A similar analysis was made in NSLS-II (Krinsky, 2005). The last may give another reason to shift the chromaticity to a positive value.

Experiences obtained in the existing LSRs running transverse feedback such as at ALS and SOLEIL demonstrate that good sharing of the tasks fighting against transverse instabilities can be made between the chromaticity shifting and transverse feedback, as long as the shifted chromaticity remains at a range that allows a bunch to exhibit predominantly dipolar motions. Such behavior of higher head-tail modes was studied in the early work of F. Sacherer (1976). The use of transverse feedback in a DLSR shall be discussed again in Subsec. 7.2.

4.2. Multibunch instabilities

4.2.1. Resistive-wall instability

As is well-known, the resistive-wall (RW) instability refers to the transverse coupled-bunch instability arising from the long range RW wake fields. Following the arguments above on the necessity for a DLSR of reducing the vacuum chamber aperture all around the ring, along with the inversely cubic dependence of the RW impedance on the aperture (Eq. 12), the RW instability is likely the most concerned instability for all DLSRs. Its impact is already quite significant in many existing LSRs, where the instability is damped either by the chromaticity shifting or transverse feedback. The instability threshold can be surprisingly low as compared to the nominal multibunch current, especially at zero chromaticity. Giving an example at SOLEIL, the threshold current is only about 30 mA vertically at zero chromaticity, while the nominal current is 500 mA, which gives a ratio of 17 between the two currents. With the radiation damping time of 6.5 ms, the above signifies that the instability growth time at 500 mA is as short as 0.4 ms, which is however still in the range that a standard transverse feedback system today can handle (Nagaoka *et al*., 2010). Because of the generally weaker dipole fields that weaken the radiation damping, the above ratio would tend to become even larger for a DLSR. It therefore becomes of great importance for a DLSR to explore means to fight against the RW instability. In particular, the shifting of chromaticity to positive is not obvious as it may excite higher-order head-tail modes and/or reduce the dynamic acceptance of the machine, causing injection and lifetime issues.

The basic behavior of the RW instability in a ring can be studied and understood to a certain degree in the frequency domain analysis using the linearized Vlasov equation, which is otherwise called the Sacherer's equation. In our formalism it reads (Laclare, 1987; Kernel, 2000)

$$i\Delta\Omega_m \cdot \sigma_m(k) \;=\; \frac{\beta_0 I \omega_0}{4\pi E/e} \sum_{k'=-\infty}^{\infty} Z_T(m_{k'}\omega_0) \cdot A^m_{kk'} \cdot \sigma_m(k'), \tag{29}$$

with

$$\begin{aligned}
\Delta\Omega_m &= \Omega_m - \omega_\beta - m\omega_s, \\
m_k &= Mk + \mu + \nu_m, \\
A^m_{kk'} &= e^{-\frac{1}{2}(\theta_k^2+\theta_{k'}^2)} I_m(\theta_k\theta_{k'}), \\
\theta_k &= \sigma\cdot(m_k - Q_\beta\xi/\alpha), \\
\sigma &= \sigma_l/R.
\end{aligned}$$

The meanings of the new symbols above are as follows,

Ω_m : Coherent angular frequency of mode m ($\nu_m = \Omega_m/\omega_0$),

M : Number of bunches (= harmonic number),

ω_s : Angular incoherent synchrotron frequency,

ω_β : Angular betatron frequency,

μ : Coupled-bunch mode number (μ = 0, 1, ..., M-1),

ξ : Chromaticity (un-normalised),

$I_m(x)$: Modified Bessel function of the order m.

The threshold is defined as the equilibrium to radiation damping, given by

$$I_{\text{th}} \;=\; \frac{4\pi E/e}{\beta_0\omega_0}\frac{1}{\tau_{rad}}\cdot\frac{1}{(\text{Im}\,\Lambda)_{\max}} \tag{30}$$

where τ_{rad} is the radiation damping time and $(\text{Im}\Lambda)_{max}$ is the largest positive imaginary part of the complex eigenvalue matrix Λ of the matrix $-i\cdot Z_T\cdot A^m$. In view of other possible sources of coherent damping, the above definition of threshold may give an underestimation. As we see in Eq. 29, the collective beam motions are characterized by two indices, m's that determine the internal bunch head-tail motions and μ's that defines the phasing among bunches. The chromaticity that enters in the A^m matrix governs the way different head-tail spectra interact with the impedance. The latter brings about similar behaviour of the threshold current as a function of the chromaticity as that in the transverse single bunch instabilities (Subsec. 4.1.3). Namely, there appears a succession of head-tail modes excitation starting from dipole, quadrupole, sextupole modes and so on driving the coupled-bunch

motions, altogether forming a threshold curve that tends to rise gradually with increasing chromaticity. A difference to the single bunch instability is that, being a multibunch instability, only multibunch harmonics separated by M times the revolution frequency count in the beam spectrum, as opposed to all revolution lines being active in a single bunch instability. It follows that an instability driving head-tail mode requires a larger chromaticity shift for it to be damped (and so its adjacent mode to become unstable).

As is also well-known, the growing transverse RW impedance at zero frequency (cf. Eq. 12) effectively makes a single coupled-bunch mode to dominate the instability when chromaticity is set to zero, namely the one situated closest to the zero frequency. This corresponds to keeping only the term with $m = 0$, $\mu = M\text{-}1$ and $k = k' = -1$ in Eq. 29, which gives

$$\tau^{-1} = \mathrm{Im}\,\Delta\Omega_0 = \frac{\beta_0\omega_0 I}{4\pi E/e}\cdot\frac{R}{b_{eff}{}^3}\sqrt{\frac{2cZ_0\rho_r}{(1-\Delta Q_\beta)\omega_0}}\ , \tag{31}$$

where b_{eff} is the effective vacuum chamber radius of the ring, ΔQ_β is the fractional part of the betatron tune and R is the machine radius as before. Equating this with the radiation damping rate $\tau_{rad}{}^{-1}$ gives an approximate expression for the RW instability current threshold at zero chromaticity, which often agrees fairly well with the observation,

$$\left(I_{th}\right)_{RW}^{\xi=0} = \frac{4\pi E/e}{c\beta_0}\cdot\frac{b_{eff}^3}{\tau_{rad}}\sqrt{\frac{(1-\Delta Q_\beta)\omega_0}{2cZ_0\rho_r}}\ . \tag{32}$$

The RW instability threshold formula above gives the well-known dependence on the fractional part of the betatron tune, indicating that the threshold current is higher when the tune is set just above an integer value.

The above simplicity at zero chromaticity is lost in the general case. One needs to solve Eq. 29 in a wide frequency space by taking into account the broadband impedance that generally gives a significant influence on the bunch coherent motions, rendering the computation difficult. An useful approximation, which was first introduced by F. Sacherer, utilises the fact that the eigensolutions of Eq. 29 are well approximated by those of the matrix $A^m_{k'k}$. Taking the eigensolution $\bar{\sigma}_{mq}(k)$ that gives the largest eigenvalue $\dfrac{C_{mq}}{\omega_0\sigma_l/c}$ (Kernel, 2000),

$$\sum_k A^m_{k'k}\bar{\sigma}_{mq}(k) = \frac{C_{mq}}{\omega_0\sigma_l/c}\cdot\bar{\sigma}_{mq}(k')\,, \tag{33}$$

one multiplies both sides of Eq. 29 by $\bar{\sigma}_{mq}(k)$ and sums over *k*. The complex coherent tune shift $\Delta\Omega_m$ of the most unstable mode is then approximately given by

$$\Delta\Omega_m \approx -i\frac{C_{mq}}{\omega_0\sigma_l/c}\frac{\beta\omega_0 I}{4\pi E/e}\frac{\sum_k Z_T(m_k\omega_0)\bar{\sigma}^2_{mq}(k)}{\sum_k \bar{\sigma}^2_{mq}(k)}. \quad (34)$$

The advantage of this method is that the eigensolutions $\bar{\sigma}_{mq}(k)$ need be computed only once, which are then stored in external files. The growth rate can then be promptly evaluated via Eq. 34. A code *rwmbi* was developed to compute the RW growth rate either fully via Eq. 29 or with the Sacherer's approximation in Eq. 34. A numerical comparison between the two methods is made by Nagaoka (2002) using *rwmbi*, where good agreement is found on the whole. Although, as usual, the above calculations in the frequency domain are limited to symmetric (uniform) beam fillings, the possibility of pursuing the dependence of the RW instability on chromaticity and broadband impedance by taking into account the head-tail degrees of freedom without involving significant computation times would keep this approach useful for a future DLSR.

For a more realistic evaluation of RW instabilities valid for partial fillings and that takes into account longitudinal collective effects such as bunch lengthening and synchrotron tune spreads, as well as nonlinear dynamics due to magnetic fields that induce additional damping of coherent motions, multi-particle tracking would be one of the most suited approaches. The code *mbtrack*, developed for this purpose, performs multi-bunch tracking using parallel computation (Nagaoka, 2006; Nagaoka, Bartolini, Rowland, 2009). It combines all the aspects of a single bunch tracking code that uses numerically deduced broadband impedance with those of a multibunch tracking code that treats long-range inter-bunch forces such as RW fields, by properly evaluating multi-turn effects. The code has recently been developed further to take into account the long-range passive harmonic cavity potential fully dynamically so to be able to simulate building up of the potential and evaluate beam transient effects (Klein *et al*., 2014). The code is being used to pursue the damping effects of the harmonic cavities against RW instability via bunch lengthening and tune spreads in MAX IV, which is the strategy adopted for MAX IV prior to employing other means such as transverse feedback or excessive chromaticity shifting (Eriksson, 2010). Multi-bunch tracking codes with similar motivations and applications for DLSRs are also developed elsewhere, such as *OASIS* (Bassi *et al*., 2012) and *elegant* (Borland, 2000).

4.2.2. HOM-induced coupled-bunch instability

HOMs (Higher-Order Modes) of the RF accelerating cavities are known to cause detrimental coupled-bunch instabilities in storage rings in the longitudinal and transverse planes, and there are quite a few LSRs that suffered from them in the past. Large efforts were therefore made in the last decades to develop normal and superconducting HOM-free cavities, which were implemented and are

successfully running in some of the recent LSRs. Since HOM-induced coupled-bunch instabilities may well limit the stored beam current or effectively blow up the transverse emittance, they should not be tolerated in a DLSR. While the RW impedance is enhanced in a DLSR, the reason of which was well discussed above as a matter practically unavoidable, it would be a pity if the performance of a DLSR is limited by cavity HOMs nowadays. For those DLSRs not implementing HOM-free cavities, it would be of great importance to assure that the HOM frequencies shall not coincide with the beam harmonics and that their instability growth rates shall be well below the radiation damping rate.

The analysis in the frequency domain can be done in a way similar to that presented in the last subsection using the Sacherer's formalism. The code *ZAP* can be used to make these calculations in both longitudinal and transverse planes (Zisman *et al*., 1986). Simple growth rate formulae, found to give good estimates for a Gaussian beam, were derived by Suzuki and Yokoya (1982). Again, a more rigorous treatment in a general beam filling in the presence of a series of different physical effects can be made with a multi-bunch tracking code such as *mbtrack* discussed above. Instead, if HOMs-induced instabilities could not be avoided in a DLSR, one of the best means to suppress them would be bunch-by-bunch feedback, in both longitudinal and transverse planes, as these instabilities would be driven by dipolar motions.

4.2.3. Ion instability

Interactions of an electron beam with ionized residual gases in a storage ring generally induce transverse center of mass oscillations of the former, effectively increasing the transverse electron beam dimensions possibly by several factors. It therefore leads to an effective emittance growth. For a DLSR, there is thus a risk of spoiling its ultimately low emittance achieved with great efforts. Though ion instabilities do not appear to be a serious issue in many modern LSRs, presumably thanks to their improved vacuum as compared to older machines, a caution may be needed for a DLSR for several reasons below. Firstly, due to a much reduced horizontal beam size, ions may be collected and interact with electrons in the horizontal plane as well, while conventionally ion instabilities occur predominantly in the vertical plane, as the transverse profile of an electron beam is usually flat in the existing LSRs. Specifically, in the linear regime, the electric field created by an electron beam having a Gaussian distribution in the two transverse planes is given by (Bassetti & Erskine, 1980)

$$E_u = \frac{\lambda}{2\pi\varepsilon_0\sigma_u(\sigma_x+\sigma_y)}\cdot u\,, \tag{35}$$

where u denotes either x or y, λ is the line density of the charge, σ_u is the rms beam size and ε_0 is the vacuum permittivity. In a DLSR, not only shall the horizontal electric field which was weak as compared to the vertical be strong and be comparable to the vertical, but the vertical field shall be even be higher due to the reduced horizontal beam size. This is to say that the overall beam sensitivity to ion instabilities shall be enhanced. The expected dependence of ion instability on the electron beam size was recently followed experimentally in SPEAR3 by L. Wang *et al*. (2013). Secondly, the generally reduced chamber aperture would lower the vacuum conductance. Whereas, the use of a distributed pumping system such as NEG coating on the vacuum chamber inner surfaces would appropriately compensate the difficulty and even suppress vacuum pressure bumps by absorbing the gases locally where they are generated. Nevertheless, during the initial vacuum conditioning phase, problems of ions are expected to appear strongly due to the low emittance nature of the electron beam mentioned above. It would be important to introduce beam gaps for ion clearing.

Not only the ion trapping, but the so called FBII (Fast Beam-Ion Instability), which is the single turn cascading interaction of a (partially filled) electron beam colliding with the residual gases and ionizing them from its head to tail of the bunch train, could be a problem for a DLSR, due again to its reduced beam dimensions in the two transverse planes. The asymptotic growth rate derived by Raubenheimer and Zimmermann (1995) for a flat beam is given by

$$\tau_{aymp}^{-1}(s^{-1}) \approx \frac{N_e^{3/2} n_b^2}{\gamma} \times \left[5 p_{gas}(\text{Torr}) \frac{r_e r_p^{1/2} L_{sep}^{1/2} c}{\sigma_y^{3/2} (\sigma_x + \sigma_y)^{3/2} A^{1/2}} \right], \tag{36}$$

where N_e denotes the number of electrons in a bunch, n_b is the number of bunches in the train, γ is the relativistic factor, p_{gas} is the residual gas pressure in torr, r_e and r_p are the classical electron and proton radii, A is the atomic mass number and L_{sep} is the bunch spacing. As pointed out in several studies including Raubenheimer & Zimmermann, (1995) and Wang *et al*., (2013), the absence of FBII in many existing LSRs despite the formula above giving sufficiently short rise times, would suggest the presence of strong damping sources in LSRs. Among which, the large variation of the beta functions and hence of the transverse beam sizes around the machine is considered to alter the ion frequency causing decoherence

$$\omega_{i,u} \approx c \cdot \left[\frac{4 N_e r_p}{3 A L_{sep} (\sigma_x + \sigma_y) \sigma_u} \right]^{1/2}. \tag{37}$$

Increasing the chromaticity should also be useful for damping with its obvious drawbacks discussed already. To fight against FBII, introduction of beam spacing between bunches is considered effective (cf. Eq. 36) and was confirmed experimentally (Wang *et al*., (2013)). Involving the bunch center of mass motions, transverse feedback should also help suppress the instability. Simulations of FBII including transverse feedback as was done by Xia, Ohmi, Elsen (2008) would be important in estimating the impact of FBII in a DLSR in advance.

While it is the vacuum pressure that rules ion instabilities, it may be worth mentioning that there can be another type of ion instability, such as the one encountered at SOLEIL, which occurs even if the pressure provided by the vacuum system may be excellent. The latter happens typically at a while (about ten minutes at SOLEIL) after reaching the final current, up to which the beam is kept completely stable at its nominal emittance with transverse feedback. The instability in most events blows up the beam, and the beam is lost completely. Experimental studies showed that, for a given total beam current, the instability can be avoided by increasing the number of bunches, namely by decreasing the bunch current, as well as by reducing the RF voltage, which means by lengthening the bunch. The conclusion drawn from which is that the concerned instability is a FBII that arises due to local outgassing brought about by beam-induced vacuum components heating. The instability appears when the FBII growth rate exceeds a certain limit defined by a transverse feedback system. A critical aspect here is that, while the ion instability should normally do nothing more than blowing up the beam to the saturation level of the beam-ion interaction, it is then transverse feedback that appears to become destructive and kills the beam. More details are discussed by Nagaoka *et al*. (2014). The fact that at SOLEIL the instability is fairly well reproduced experimentally under the same condition and constantly existed at all times implies that it concerns a vacuum element that has a steady response to the beam. Vacuum experts at SOLEIL suspect in-vacuum insertion devices among different candidates (Herbeaux, 2014). Currently there are ten such devices installed at SOLEIL. A similar beam instability observation was made recently at SSRF (Shanghai, China) as a function of an in-vacuum insertion device gap, in the presence of transverse feedback (reported by Nagaoka *et al*., 2014). Being a phenomenon involving RW instability, transverse feedback, beam-induced heating and FBII, and deeply related to the fact of having reduced chamber aperture, such instability could become a serious concern for a future DLSR. Again, bunch lengthening via harmonic cavities may be an effective means of mitigating the instability.

5. IBS and Touschek scattering

Intra-beam scattering (IBS) describes multiple Coulomb scattering that in electron machines leads to an increase in all bunch dimensions and in energy spread, whereas the Touschek effect concerns large single Coulomb scattering events where energy transfer from transverse to longitudinal leads to

immediate particle loss. In low emittance machines, such as DLSRs, both effects tend to be important: IBS will limit the emittances that can be achieved and the Touschek effect sets the beam lifetime.

5.1. IBS (Intra-Beam Scattering)

A. Piwinski (1974) was one of the first to come up with a systematic solution for the IBS growth rates in storage rings. In recent times, however, an alternate formulation by Bjorken & Mtingwa (1983) is typically used in simulation programs, such as *MAD* and *elegant*. Through tests and analysis it is believed that the results of the two formalisms normally are in good agreement. Solving the Bjorken-Mtingwa (BM) equations can be time consuming, so S. Nagaitsev (2005) developed an algorithm that can speed up the calculation by an order of magnitude. Kubo & Oide (2001) recast the BM equations so that the three degrees of freedom (horizontal *x*, vertical *y*, and energy *p*) are treated on equal footing, and the couplings between them are included in a natural way; the method is installed in the optics program *SAD* (Oide, 1986). All these methods assume Gaussian bunch distributions, of which they find the second moments. However, recently there has been an effort to simulate IBS via Monte Carlo methods, in order to investigate the non-Gaussian nature of the steady-state bunch distributions (see e.g. Vivoli & Martini (2010)).

The IBS calculations of the steady-state emittances ε_x and ε_y, and (relative) energy spread σ_p are normally performed by simultaneously solving

$$\varepsilon_x = \frac{\varepsilon_{x0}}{1-\tau_x/T_x}, \qquad \varepsilon_y = \frac{\varepsilon_{y0}}{1-\tau_y/T_y}, \qquad \sigma_p^2 = \frac{\sigma_{p0}^2}{1-\tau_p/T_p}, \tag{38}$$

with subscript 0 indicating a nominal, zero current value; where τ_i indicates the synchrotron radiation damping times, and $1/T_i$ the averaged IBS growth rates (in amplitude), for the three directions. Note that the local IBS growth rates $\delta(1/T_i)$ are functions of beam properties and local lattice functions. These rates are calculated for all positions around the ring and then averaged ($\langle\ \rangle$ means to average around the ring) to give $\langle\delta(1/T_i)\rangle = 1/T_i$, and then Eqs. 1 are solved simultaneously. Note that since the growth rates also depend on the beam emittances, energy spread, and bunch length, Eqs. 38 need to be solved by iteration.

A simplified model of the BM equations that can be used to approximate the more accurate BM equations for typical rings is the so-called “high energy approximation” (K. Bane, 2002). We present it here since it may more clearly show the parameter dependence of IBS than the other, more rigorous formulations. According to this model the IBS growth rate in energy spread is given by

$$\frac{1}{T_p} \approx \frac{r_e^2 c N_e (\log)}{16\gamma^3 \varepsilon_x^{3/4} \varepsilon_y^{3/4} \sigma_z \sigma_p^3} \left\langle \sigma_{\mathrm{H}}\, g(a/b)\, (\beta_x \beta_y)^{-1/4} \right\rangle. \tag{39}$$

Here r_e is the radius of the electron, c the speed of light, N_e the number of electrons per bunch, (log) the Coulomb log factor, γ the Lorentz energy factor, σ_z the bunch length, and β_x, β_y, the optical beta functions. Other factors in Eq. 39 are defined by

$$\frac{1}{\sigma_H^2} = \frac{1}{\sigma_p^2} + \frac{\mathcal{H}_x}{\varepsilon_x}, \quad a = \frac{\sigma_H}{\gamma} \sqrt{\frac{\beta_x}{\varepsilon_x}}, \quad b = \frac{\sigma_H}{\gamma} \sqrt{\frac{\beta_y}{\varepsilon_y}}, \tag{40}$$

$$g(\alpha) = \alpha^{(0.021 - 0.044 \ln \alpha)}, \tag{41}$$

where $\mathcal{H} = [\eta^2 + (\beta\eta' - \beta'\eta/2)^2]/\beta$ is the dispersion invariant. Finally, the horizontal IBS growth rate (in amplitude) is given by

$$\frac{1}{T_x} = \frac{\sigma_p^2}{\varepsilon_x} \left\langle \mathcal{H}_x \delta(1/T_p) \right\rangle. \tag{42}$$

Finally, note that the high energy IBS approximation given here has validity when a, b << 1, which holds for typical light sources.

In scattering calculations, like IBS, a Coulomb log term is typically used to take into account the contribution of very large and very small impact parameter events. Due to the very small impact parameter events, the tails of the steady-state bunch distributions are not Gaussian and the standard way of computing (log) overemphasizes their importance. To better describe the size of the core of the bunch, T. Raubenheimer (1994) proposed a method that reduces the Coulomb log factor (Kubo & Oide, 2001). For a typical DLSR like PEP-X, the Coulomb log becomes (log) ~ 10.

We now present example calculations for the case of PEP-X, a DLSR project that uses round beams to weaken IBS (Cai *et al.*, 2011). Selected parameters of PEP-X are given in Table 2. Before beginning IBS calculations, one needs to know the source of the vertical emittance; specifically, what

is the combination of vertical dispersion and coupling? For the PEP-X calculations, for simplicity, it was assumed that the machine was coupling dominated. Note, however, that in practice, using coupling to generate round beams may not be the best strategy.

If we are coupling dominated, then the vertical emittance is proportional to the horizontal emittance, and we can write

$$\varepsilon_x = \frac{\varepsilon}{1+\kappa} \quad \text{and} \quad \varepsilon_y = \frac{\kappa\varepsilon}{1+\kappa}, \tag{43}$$

with κ the coupling constant and $\varepsilon = \varepsilon_x + \varepsilon_y$ the sum emittance. The nominal (no IBS) horizontal and vertical emittances are given by $\varepsilon_{x0} = \varepsilon_0/(1 + \kappa)$ and $\varepsilon_{y0} = \kappa\,\varepsilon_0/(1 + \kappa)$, where ε_0 is a property of the lattice.

Table 2
A selection of PEP-X parameters

Parameter	Value	Units
Energy, E	4.5	GeV
Circumference, C	2199	m
Average current, I	200	mA
Bunch charge, eN_e	0.45	nC
Relative rms energy spread, σ_{p0}	1.1	10^{-3}
Rms bunch length, σ_{z0}	3.0	mm
Nominal emittance sum, ε_0	10.95	pm
x-y coupling parameter, κ	1	

We make the assumption that the transverse growth rate can be approximated (Cai *et al*., 2011)

$$\frac{\varepsilon_{x0}}{\tau_x} + \frac{\varepsilon_{y0}}{\tau_y} - \frac{\varepsilon_x}{\tau_x} - \frac{\varepsilon_y}{\tau_y} + \frac{\varepsilon_x}{T_x} = 0. \tag{44}$$

The first two terms in Eq. 44 represent quantum excitation growth rates, the next two terms those of radiation damping, and the last term that of IBS. (A similar equation applies for the growth in p.)

Then IBS calculations of the steady-state emittance ε and (relative) energy spread σ_p are performed by simultaneously solving

$$\varepsilon = \frac{\varepsilon_0}{1-\tau_x^*/T_x} \quad \text{and} \quad \sigma_p^2 = \frac{\sigma_{p0}^2}{1-\tau_p/T_p}, \tag{45}$$

where $\tau_x^* = \tau_x/(1 + \kappa\tau_x/\tau_y)$. In this manner, BM IBS calculations were performed for PEP-X with the parameters of Table 1. The results are shown in Table 3, where the zero current and nominal current beam properties are given. We note that for PEP-X, IBS has little effect on σ_p and σ_z; however, at the nominal current, ε_x has doubled from the zero-current value. We can imagine that it is IBS (and the goal of being diffraction limited in both planes) that sets the choices of I = 200 mA and round beams for PEP-X. In more detail we find that the horizontal IBS growth rate at steady-state is T_x^{-1} = 52 s^{-1}; the high energy approximation yields T_x^{-1} = 54 s^{-1}, in reasonable agreement to the Bjorken-Mtingwa solution. In Fig. 14 we plot the emittances $\varepsilon_x = \varepsilon_y$ as functions of current I.

Table 3
For PEP-X: steady-state emittances, energy spread, and bunch length at zero and nominal currents.

I [mA]	ε_x [pm]	ε_y [pm]	σ_p [10^{-3}]	σ_z [mm]
0	5.5	5.5	1.10	3.00
200	11.5	11.5	1.15	3.15

Further IBS calculations were performed for the PEP-X lattice, but now allowing the energy of the machine to change through scaling (Cai *et al*., 2011). In Fig. 15 we plot emittance vs. machine energy, at zero current and near nominal current. At nominal current, at low energies IBS becomes stronger and at high energies synchrotron radiation becomes stronger, with the minimum emittance obtained at E = 5 GeV. We see that the chosen PEP-X energy is near-optimal.

5.2. Touschek Scattering

In low emittance machines, such as DLSRs, the Touschek effect sets the beam lifetime. Transverse scattering leads to large energy kicks for some particles; these particles, in turn, perform betatron oscillations and are soon lost on the physical or dynamic aperture. Generally, as the beam emittances are reduced, the Touschek lifetime drops. However, for the very small emittances that are found in some DLSRs, the Touschek lifetime begins to rise again. This is understood in the following way: since the Touschek effect is initiated by transverse scattering, the cooling of the beam transversely ---

the reduction of the emittances --- will eventually reduce the scattering and begin to increase the beam lifetime.

Touschek lifetime calculations normally follow the flat-beam equation of Bruck (1966), with modifications by Piwinski (2006). Some DLSR projects, like PEPX, are considering round beams in order to weaken IBS and thus achieve lower emittances. One can always use the more general formula due to Piwinski (2006, 1999). With the Touschek effect the number of particles in a bunch decays with time *t* as

$$N_e = \frac{N_{e0}}{1+t/\mathcal{T}}, \tag{46}$$

with N_{e0} the initial bunch population, and $\mathcal{T}$ the Touschek lifetime. Note that the decay is not exponential. The lifetime is given by (Piwinski, 2006)

$$\frac{1}{\mathcal{T}} = \frac{r_e^2 c N_e}{8\sqrt{\pi}\beta^2\gamma^4\sigma_z\sigma_p\varepsilon_x\varepsilon_y}\left\langle \sigma_H \mathcal{F}(\delta_m)\right\rangle, \tag{47}$$

with

$$\mathcal{F}(\delta_m) = \int_{\delta_m^2}^{\infty} \frac{d\tau}{\tau^{3/2}}\, e^{-\tau B_1}\, I_0(\tau B_2)\left[\frac{\tau}{\delta_m^2} - 1 - \frac{1}{2}\ln\left(\frac{\tau}{\delta_m^2}\right)\right] \tag{48}$$

$$B_{1,2} = \frac{1}{2\beta^2\gamma^2}\left|\frac{\beta_x\sigma_x^2}{\varepsilon_x\tilde{\sigma}_x^2} \pm \frac{\beta_y}{\varepsilon_y}\right|, \tag{49}$$

where $\langle\ \rangle$ indicates averaging around the ring. In this formula the only assumptions are that there is no vertical dispersion and that the energies are non-relativistic in the beam rest frame ($\gamma^2\sigma_x^2/\beta_x^2$, $\gamma^2\sigma_y^2/\beta_y^2 << 1$); there is no requirement that the beam be flat. Parameters are average velocity over

the speed of light β, modified Bessel function of the first kind I_0, relative momentum acceptance δ_m (half aperture), and beam sizes $\sigma_x = \sqrt{\beta_x \varepsilon_x + \eta_x^2 \sigma_p^2}$ and $\tilde{\sigma}_x = \sqrt{\beta_x \varepsilon_x + \beta_x \mathcal{H}_x \sigma_p^2}$ ($\mathcal{H} = [\eta^2 + (\beta\eta' - \beta'\eta/2)^2]/\beta$ is the dispersion invariant and σ_H is defined in Eq. 40). Because of the cut-off factor $exp(-\tau B_1)$ in the integral of Eq. 48, with $B_1 \sim \beta/\varepsilon$: (i) the Touschek effect is strongest where the beam size is small and (ii) the effect becomes weak again for very small emittances. The Touschek lifetime depends on the momentum acceptance of a ring, $\delta_m(s)$, which can be obtained in the following manner: in tracking around a ring, at a given position s a beam particle is given a relative (positive) momentum kick $\delta_m(s)$, and it undergoes betatron oscillation. The largest value of δ_m for which the particle survives a few turns defines the positive momentum aperture at position s. Then the same is done for a negative momentum kick.

We now show some example plots for the case of PEP-X, a DLSR project that uses round beams (Cai *et al*., 2011). For PEP-X the momentum acceptance is limited in the bends (where the beam size is small), with a typical value $\delta_m \sim \pm 3\%$. Performing the Touschek lifetime calculations --- based on the numerically obtained $\delta_m(s)$ and on the IBS determined, steady-state beam sizes --- one finds that $\mathcal{T}$ = 12 hours. Touschek liftetime calculations were also performed for the PEP-X lattice, as a function of global acceptance parameter δ_m (with the momentum aperture everywhere given by $\pm\delta_m$) (see Fig. 16, the blue symbols). The curve in the plot gives a fit to the calculations: $\mathcal{T} = 0.088(\delta_m/0.01)^5$. One can see that the Touschek lifetime is a very sensitive function of momentum aperture: at $\delta_m = 2\%$ the lifetime is only ~ 2 hours. In PEP-X damping wigglers, of nominal length $L_w = 90$ m, are also used in reducing the emittance. In Fig. 17 we plot ε_x and $\mathcal{T}$ (normalized to their values when $L_w = 90$ m) vs. L_w. These results are self-consistent calculations including IBS. We see that, over most of the range, as the emittance decreases, the Touschek lifetime indeed increases, though only gradually.

6. Other collective effects

Up to this point, we have reviewed the collective beam instabilities and particle scattering that may potentially give a significant impact in a DLSR. In addition to which, there are at least two other beam intensity-dependent phenomena that may become a concern, even if the former are well kept under control. The first is the beam-induced vacuum components heating, and the second, the incoherent betatron tune shifts arising either from vacuum chambers having non-circular cross sections or from space-charge.

6.1. Beam-induced machine heating

As is well-known, the wake field excited by a beam in a vacuum chamber may de-accelerate the latter, rendering the beam to deposit a part of its energy in the beam duct, which may convert to heat in the chamber. The amount of energy deposited can be described in terms of the loss factor $\kappa_{//}(\sigma)$ in Eq. 6, in which the real part of the longitudinal impedance $\mathrm{Re}Z_{//}(\omega)$ can be seen to be the origin. Although many vacuum components exhibit non-zero $\mathrm{Re}Z_{//}(\omega)$ only above the vacuum chamber cut-off frequency, it implies that a short bunch in a DLSR has more chance of interacting with them. Potentially risky vacuum components in a DLSR would be flanges, BPMs, shielded bellows, taper transitions and ceramic chambers for pulsed magnets, as were listed in Subsec. 3.2 as important impedance contributors in a DLSR. Referring again to the SOLEIL flange, though the RF shielding with a metallic foil prevents well from the flange getting heated, in reality it may happen that the metallic sheet gets deteriorated from its original shape and position, due for example to occasional vacuum interventions. At SOLEIL a number of flanges had to be repaired due to beam-induced excessive temperature rise originating from the above deterioration in the RF shielding. This example indicates the importance of studying the extent to which the impedance may be degraded due to deformation of chamber components.

The problem of beam-induced heating was a serious concern in the other example of the SOLEIL BPM described in Subsec. 3.2 with its trapped mode as well, since the possible dilation of the buttons as a consequence can deteriorate the orbit reading accuracy, which would be a more critical issue for a DLSR. In this case, one must not only evaluate the loss factor, but see how much of the energy lost by the beam goes into the buttons. A post-processing routine of *GdfidL* was used to evaluate the Joule loss through the surface integral

$$P = \iint \frac{H_{//}^2}{(2\kappa\delta)} dF \quad [\mathrm{W}] \tag{50}$$

where $H_{//}$ is the tangential magnetic field obtained in the wake potential calculation, κ is the conductivity of the materials involved and δ is the skin depth at the trapped mode frequency. By assuming in one case that the BPM block surrounding the button is superconducting, a half of the Joule loss was concluded to arise from the button. When dealing with a long lasting wake field such as a trapped mode, the calculation of the loss factor needs be extended to include the coupled-bunch effect through the expression

$$k_{loss} = \frac{1}{\pi} \sum_{m=0}^{\infty} \int_{0}^{\infty} e^{-\sigma_l^2 \omega^2 / c^2} \cdot \left[\mathrm{Re}\, Z_{//}(\omega) \cdot \cos(m\Delta T \omega) + \mathrm{Im}\, Z_{//}(\omega) \cdot \sin(m\Delta T \omega) \right] d\omega \qquad (51)$$

where ΔT denotes the RF period. Here, it is important to correctly evaluate the quality factor of the resonant mode. In the above example, an effective damping time of the trapped mode was estimated by equating the wall energy loss integrated over time to the single bunch energy loss, and then defined the resonant Q-value accordingly. Approximately three RF period was concluded. The formula above gave an increase of the loss factor by more than a factor of three as compared to the uncoupled case in the worst case when the trapped mode is in resonance with the RF (Nagaoka *et al*., 2006).

6.2. Incoherent tune shifts

As PWD (Potential Well Distortion) in the longitudinal plane, a beam in the storage ring could generate a quadrupolar wake potential, under specific conditions, which modifies the betatron tunes of the individual electrons. There may be two possibilities for a DLSR: One is due to vacuum chambers having non-circular cross sections, and the other due to the space-charge force of a beam itself. Looking firstly from the former, we recall that a usual dipolar transverse wake $W_{\perp}$ is created when the bunch center of mass is displaced from the origin, which is true even if the chamber cross section is circular. Now if instead the chamber cross section is non-circular, a transverse wake field is created even if the beam traverses on-axis, in which the primary multiple content is known to be quadrupolar. For a chamber having a cross section with larger width than height, the quadrupole component is focusing in x and defocusing in y. With resistive-walls (RWs), the generated wake is a long-range quadrupolar field which is superimposed over many turns to introduce effective quadrupoles in the ring that depend linearly on the beam current. The effect was studied by several groups (Gluckstern *et al*., 1992; Yokoya, 1993; Burov & Lebedev, 2002). The dependence of the quadrupole wake on an arbitrary chamber cross section was studied by Yokoya (1993). While the long range nature of RW field creates the above linear dependence of the focusing strength on the total beam current which can be easily measured in terms of average tunes, the short-range RW field, which is much larger in amplitude, introduces non-uniformity in the tune shift along a bunch train. In particular, incoherent tune shifts can be much larger for a particle in a high intensity bunch. For a flat chamber, due to the relation $(Z_H)_{incoherent} = -(Z_H)_{coherent}$ that holds, the average focusing strength in a bunch may be given by (Nagaoka, 2004),

$$< k_{effs} > = \frac{4\pi}{Q} \cdot \frac{1}{E/e} \int_0^\infty \tilde{\lambda}(\omega)^2 \cdot \mathrm{Im}\, Z_H(\omega)\, d\omega \quad [\mathrm{m}^{-1}]. \tag{52}$$

On the other hand, the importance of field diffusion through a finite thickness RW that determines the effective duration of the exited field in predicting the tune shift due to the long range RW, was pointed out by Chao, Heifets, Zotter (2002). Such field decay may be approximated by that in a circular RW chamber of thickness *t* given by

$$\left[W_\perp^{RW}(s)\right]_{thin\,wall} = \frac{c\rho_r}{\pi b^3 t} \exp\left(-\frac{\rho_r}{rbtZ_0} \cdot s\right) \quad [\mathrm{V/C/m}^2], \tag{53}$$

where *t* is the chamber wall thickness, $r = 1-(b/d)^2$, and *b* and *d* are respectively the inner and outer chamber radius. Incoherent tune shifts arising from non-circular cross section chambers were observed and reported from several machines such as ESRF, BESSY-II, PEP-II HER, and SOLEIL (Nagaoka *et al*., 2000; 2002; Chao, Heifets, Zotter, 2002; Brunelle *et al*., 2014). In magnitude, they can reach several 10^{-2} level between zero and the maximum stored beam current. The recent measurement done at SOLEIL using a precise orbit response matrix analysis could in particular identify the location of low gap flat chambers along the ring with good linear dependence of the deduced focusing strength on the beam current (Brunelle *et al*., 2014). In view of furthermore reduced vacuum chamber apertures, the incoherent tune shifts due to non-circular chambers are expected to be larger for a DLSR. Owing to specific technical reasons such as accommodation of octupole magnets or to the simplicity of NEG coating, however, circular cross section chambers were adopted for MAXIV 3 GeV ring in the magnet sections (Al-Dmour *et al*., 2011), and other DLSRs such as Sirius (2013), ESRF-II and APS-II seem to follow the same trend. From the viewpoint of minimizing the undesired tune shifts, the use of circular cross section chambers is clearly favorable for a DLSR.

Looking now at the incoherent space-charge tune shift, the underlying force arises from the electro-magnetic field created by the ensemble of electrons in the same bunch. As well-known, for relativistic electrons, the field is confined in a disk traversing longitudinally with an opening angle γ^{-1}. Since the electric field tends to cancel with the magnetic field only leaving a residual that depends on γ^{-2}, the effect is usually negligible for LSRs, which however may not be true for a DLSR due to much smaller transverse beam dimensions. The maximum tune shift at the peak density of a bunch having Gaussian distributions in all three planes is given by (Wolski, 2009)

$$\Delta\nu_u = -\frac{r_e i_b T_0}{(2\pi)^{3/2} e\sigma_l \gamma^3} \oint \frac{\beta_u}{\sigma_u(\sigma_x+\sigma_y)} ds \tag{54}$$

where u denotes either x or y, r_e is the classic electron radius, i_b the bunch current, T_0 the revolution period, β_u the betatron function in the plane u, and the integral over s extends around the ring. While the former effect due to non-circular cross section chambers acts on the tunes of all particles by explicitly distorting the machine optics, the latter only affects those that are in a highly charged bunch. Making an estimate of the order of magnitude, the tune shifts may equally reach 10^{-2} level as the former for some of the upcoming DLSRs. A difficulty associated in both effects is that there shall simultaneously be tune "spreads" arising from local charge density variations, though the latter may be beneficial against collective effects. Thus, while a system of tune feedback could restore the average tunes of the machine, there can be significantly detuned particles. Due to the enhanced sensitivity of the single particle dynamics (e.g. on and off-momentum apertures) anticipated in a DLSR due to stronger focusing, the above incoherent optics distortion arising from current ramping or in-vacuum insertion device gap closure may lead to undesirable performance degradation, such as emittance increase, reduction of injection efficiency and beam lifetime. It may become an issue especially for low and medium energy machines.

7. Cure of beam instabilities in a DLSR

Having reviewed collective beam instabilities that are likely to appear in a DLSR, let us now see what measures could be taken to alleviate or fight against them. Our discussions shall be based on the experiences obtained in the existing 3rd generation light sources as well as simulations carried out on some of the future DLSRs.

7.1. Chromaticity shifting

A shift of the chromaticity to positive helps damp a unstable head-tail mode thanks to the so-called head-tail damping. The theory explains that the shift brings the head-tail mode spectrum to better overlap with the positive frequency part of $ReZ_\perp(\omega)$ that induces coherent damping than the negative frequency part that has the opposite effect. The chromaticity shifting should be effective in stabilizing a single bunch against TMCI or head-tail instability, as well as a multibunch beam against resistive-wall instability. The possible limitation, however, is that at the cost of damping a head-tail mode, the shift may excite higher-order modes that were previously stable. Although it is generally true that the impact of a high-order mode excitation is smaller, the beam can still be lost. The chromaticity shifting

does not therefore guarantee beam stabilization by itself. Besides, as well-known, a larger positive chromaticity generally signifies stronger sextupoles, thus increasing the nonlinearity of the machine optics and reducing the dynamic acceptance. The latter creates a serious issue for a DLSR in particular that inherently suffers from a small dynamic acceptance. The chromaticity shifting should therefore be used moderately, possibly in combination with other means as discussed below, so to be able to operate the ring with a small enough chromaticity. Giving an example at SOLEIL, the chromaticity shifting is combined with transverse feedback, thanks to the fact the quadrupolar and sextupolar head-tail modes excited still exhibit strong enough dipolar-like motions (Sacherer, 1976). The value of chromaticity is optimized according to the beam filling patterns and the total beam current that characterize the head-tail mode excitation. In particular, zero chromaticity is avoided due to enhancement of FBII (Fast Beam-Ion Instability).

7.2. Bunch-by-bunch feedback

For collective instabilities associating dipolar motions, whether transverse or longitudinal, bunch-by-bunch feedback appears to be a highly efficient method of stabilizing the beam with today's advanced technology in digital signal processing. It may therefore be considered as indispensable for a DLSR, especially in view of its low resistive-wall (RW) instability threshold. Indeed, with the commercially available FPGA-based digital boards, turn-by-turn and bunch-by-bunch feedback has become a standardized tool that can be installed in a storage ring and commissioned relatively simply (Nakamura & Kobayashi, 2005; Plouviez *et al*., 2008; Morgan, Rehm, Uzun, 2008; Nagaoka *et al*., 2010). All we need in addition are practically a pair of a wideband detector and a deflector. The programmability of a FPGA board allows installing the latter equipment at arbitrary locations in the ring, as well as coping with machine optics changes. SOLEIL is among the modern light sources in which transverse bunch-by-bunch feedback is running routinely against all beam filling modes that require it, whether the instability is of multibunch or single bunch nature (Nagaoka *et al*., 2010). It allows pushing the resistive-wall threshold of around 30 mA at zero chromaticity to above 500 mA, its highest nominal current. Transverse feedback manages to maintain the vertical emittance to the nominal value of 40 pm without spoiling it even though the beam instability is existing predominantly in this plane. In this respect, the smallness of the horizontal emittance in a DLSR would not be an issue for transverse feedback. Since the radiation damping time is nearly 6 ms, it signifies that the feedback damping time is shorter than 0.36 ms at the latter current. In addition, storage of bunch-by-bunch and turn-by-turn center of mass and deflection data allows good analysis of the beam instability. Data analysis at SOLEIL shows that transverse feedback stabilizes beam against both RW and ions simultaneously in the high current multibunch operation. In single bunch, the TMCI threshold is increased by nearly a factor of three with the maximum stripline power available. Whereas with the chromaticity of ~2, the head-tail instability threshold found at ~5 is pushed up to

beyond 20 mA. ALS reported having achieved a much higher factor of gain than three against TMCI, limited by other machine constraints (Byrd, 2014).

7.3. Bunch lengthening with harmonic cavities

The idea of adding cavities running at a higher-harmonic (usually around third harmonic) of the main RF frequency in a storage ring is to superimpose its potential to that of the original cavity such as to make the sum of the two potentials flat around the synchronous phase, thereby elongating an electron bunch (Hoffmann & Myers, 1980; Byrd, 2014). It is an effective way of improving the beam lifetime of low to medium energy low emittance LSRs that suffer from short Touschek lifetime. In addition to bunch lengthening, the flattened potential also induces synchrotron tune spread which in turn helps stabilizing the beam against collective instability. The storage rings such as ALS, BESSY-II, SLS and ELETTRA have successfully made use of them in improving the lifetime, and some of them have also experienced in fact damping of longitudinal coupled-bunch instability excited by cavity HOMs (Byrd & Georgsson, 2001; Anders & Kuske, 2003; Pedrozzi *et al*., 2003; Svandrlik *et al*., 2003). As far as a high peak current or a short bunch length operation is not intended, active lengthening with harmonic cavities should therefore be a very helpful means for a DLSR to attain its target performance, in terms of emittance, beam current, lifetime, by mitigating collective effects, IBS and Touschek scattering. Simulation studies are underway for NSLS-II, MAXIV and Sirius by including passive harmonic cavities in the multi-particle tracking, whose potential is dynamically loaded by the beam (Bassi *et al*., 2012; Klein, M. *et al*., 2014). In this way, the transient beam loading is well taken into account in the arbitrary filling simulated. The former two address as well the question on the possible stabilization of transverse instability due to harmonic cavities through bunch lengthening and synchrotron tune spread. Advanced multibunch tracking codes are developed for this purpose that track bunches consisting themselves of a large number of macro particles. Both long-range inter-bunch and short-range intra-bunch forces are simultaneously treated using parallel computation on a large cluster of processors (Klein, M. *et al*., 2014). In particular, resistive-wall wakes are stored over multi-turns to achieve appropriate convergence in summations. The on-going study for MAXIV attempts to clarify the effectiveness of the strategy set up (Eriksson, 2011) in mitigating the resistive-wall instability with a combination of harmonic cavities and chromaticity shifting, without *a priori* depending on transverse feedback, in view of both the narrowing of the head-tail spectra with bunch lengthening and the rapidly decaying amplitude of the higher-order head-tail modes (Fig. 18). Regarding the choice between active and passive harmonic cavities, it would clearly be advantageous have active cavities for a DLSR that delivers high current bunches without necessarily having a high total current such as a few bunch mode, while passive cavities may be more adapted for those that would exclusively deliver high multibunch currents, especially from the power saving point of view. To avoid complications of the cavity tuning at an intermediate beam current during beam ramp, however,

it may be advantageous for a passive system to keep nevertheless the possibility of feeding power to the cavities externally (Tavares, P.F., 2014).

8. Conclusion

In this paper we have seen that efforts to achieve and store an ultra-low emittance beam in a diffraction limited storage ring (DLSR) tend to enhance beam collective effects simultaneously in several distinct ways. Firstly, the strong magnetic focusing of the beam in the ultra-low emittance optics requires magnet bore radii and hence vacuum chamber aperture to be reduced as compared to conventional machines, which directly results in enhancing the machine coupling impedance. Secondly, the storage ring, due to its reduced horizontal dispersion in the ultra-low emittance optics becomes furthermore isochronous, as indicated by its relatively low momentum compaction factor, rendering the natural bunch length shorter and the beam more sensitive to single bunch instabilities. In addition, the beam with its wider bunch spectrum couples more easily to high frequency impedance, again increasing the source of instability. Thirdly, the fact of having ultra-small transverse dimensions renders the beam more sensitive to Coulomb scattering as the number of particles is raised within a bunch, resulting in an emittance blow-up and likely in a reduction of Touschek lifetime. Besides, we have also seen that other collective effects, such as bunch lengthening, beam-induced machine heating and incoherent and coherent tune shifts generally tend to get stronger as well.

Despite the general trend that we have seen above for DLSRs, the gravity of the collective effects would depend on the specificity of a DLSR, above all on its mode of operation such as the designed beam intensity and the beam filling pattern. For example, if the machine is merely operated in a multibunch mode, the impact of short-range wake fields as well as bunch current-dependent effects such as IBS and Touschek scattering would be less influential. On the other hand, if a machine is intended to be operated in several different filling patterns including single or a few bunch modes, minimization of broadband impedance would be a particularly important issue. Naturally, the energy of the machine is a key parameter in defining the beam sensitivity to collective effects. For example, incoherent tune shifts arising from non-circular chambers may not be a serious issue for a high energy machine since the beam would be much less sensitive to optical perturbations generated by insertion devices.

Measures to mitigate the above collective effects in a DLSR would also depend on the specificity of each machine. If a short bunch is not an option in the operation, active bunch lengthening with harmonic cavities (either passive or active) would be a good solution, as it may not only be effective in suppressing certain beam instabilities and beam-induced machine heating, but also relax IBS and Touschek effects. The latter benefit would be particularly important for a DLSR. Whereas, transverse bunch by bunch feedback could be a good option for all DLSRs aiming to run at high single and

multibunch current, in view of its successful and reliable operation demonstrated in several existing light sources. In fact, we may even be able to go one step further to relax our choice of the vacuum chamber material and choose one that has high electric resistivity but possessing, for example, better gas desorption or SR irradiation properties. Transverse feedback also provides the known advantage of enabling to run the machine at reduced or zero chromaticity, which would be particularly important for a DLSR. Its continuous performance upgrade, in terms of reactivity, higher bandwidth and higher kick amplitude, would be well appreciated in running a DLSR both in multibunch and high bunch intensity operations.

Though we have put emphasis on the importance of transverse feedback in this paper in view of the resistive-wall and head-tail instabilities that appear difficult to circumvent, one must not forget the risk of encountering longitudinal beam instabilities. The above may typically arise from vacuum components capable of inducing high Q wakes such as RF cavities with their Higher-Order Modes (HOMs). Careful analysis of the impedance of such objects must therefore be made, as well as assessment of the need of longitudinal feedback. Likewise, the choice of a RF system, such as its operating frequency in connection with the envisaged operation schemes, whether normal or super-conducting, and whether or not HOM-free, must thoughtfully be made, as it will likely have a significant impact on the beam stability.

Lastly, efforts to understand the physical mechanism of beam instability or oppositely the stabilization mechanism must still be continued for several concerned problems. In view of the THz users in the SR community, CSR instability must be explored in more detail such as on the vacuum chamber dependence, the long range coupled-bunch effects, or in combination with the beam dynamics in the negative momentum compaction regime. Different sources of instability stabilizing (Landau damping) effects such as those provided by harmonic cavities in both longitudinal and transverse planes, or by the optics nonlinearity (higher-order amplitude-dependent tune shifts and higher-order chromaticity) need be investigated. The high frequency impedance or very short-range wake fields of various vacuum chamber components in a DLSR, which may be the dangerous sources of harmful single bunch instabilities such as microwave or TMCI and head-tail, must be pursued in more detail. The new semi-analytical method described in Subsec. 3.2 may become a powerful alternative approach as opposed to intensive numerical wake potential calculations. With the computing power available today, the multibunch tracking taking simultaneously the single bunch degrees of freedom into account such as that described in Subsec. 7.3 would be an effective way of elucidating the underlying beam physics that are not fully understood yet. The advances in the studies of beam collective effects would allow us to better optimize the future DLSRs towards their ultimate performance.

Acknowledgements One of the authors, (R.N.) thanks Marit Klein, Galina Skripka, Pedro F. Taveres, Christian Herbeaux, Henrique de Oliveira Caiafa Duarte, Rafael Molena Seraphim and Michael Hahn for their help in creating this manuscript.

References

Agoh, T., Yokoya, K. (2004). Phys. Rev. ST Acell. Beams **6**, 054403.

Al-Dmour, E. et al., (2011). *Vacuum System Design for the MAX IV 3 GeV Ring*, Proc. of IPAC2011, San Sebastian, Spain, 1554.

Anders, W., Kuske, P. (2003). *HOM Damped NC Passive Harmonic Cavities at BESSY*, PAC03, Portland, Oregon.

Bane, K., Sands, M. (1987). *Wakefields of Very Short Bunches in an Accelerating Cavity*, SLAC-PUB-4441.

Bane, K., Sands, M. (1995). *The Short-Range Resistive Wall Wakefields*, SLAC-PUB-95-7074.

Bane, K.L.F. (2002). *A Simplified Model of Intrabeam Scattering*, EPAC02, Paris, p. 1443.

Bane, K.L.F., Stupakov, G., Zagorodnov, I. (2007). Phys. Rev. ST Accel. Beams **10** 074401.

Bane, K.L.F., Cai, Y., Stupakov, G. (2010). Phys. Rev. ST Accel. Beams **13** 104402.

Bane, K. (2013). *Review of Collective Effects for Low Emittance Rings*, talk given at LER workshop, Oxford, UK, July 2013.

Bane, K. (2014). *Review of CSR Instabilities in Electron Storage Rings*, talk given at TWIICE workshop, Synchrotron SOLEIL.

Bassetti, M., Erskine, G.A. (1980). *Closed expression for the Electrical Field of a Two-Dimensional Gaussian Charge*, CERN-ISR-TH/80-06.

Bassi, G. et al. (2012). *Passive Landau Cavity Effects in the NSLS-II Storage Ring*, IPAC2012, 1701, New Orleans, Louisiana.

Bjorken, J. D., Mtingwa, S. K. (1983). Particle Accelerators, **13**, 115.

Blednykh, A. (2014). *Impedance Analysis of Insertion Devices*, talk given at TWIICE workshop, Synchrotron SOLEIL.

Borland, M. (2000). *ELEGANT: A flexible SDDS-compliant code for accelerator simulation*, http://www.osti.gov/scitech/biblio/761286.

Borland, M. (2014). Private communication, APS, Argonne, Illinois.

Boussard, D. (1975). CERN Report LABII/RF/INT/75-2 (1975).

Bruck, H. (1966). *Accélérateurs Circulaires de Particules; Introduction à la Théorie, Saclay*.

Brunelle et al. (2014). *Impact of Incoherent Transverse Wakefield on Storage Ring Optics*, talk given at TWIICE workshop, Synchrotron SOLEIL.

Bruns, W. (1996). *The GdfidL Electromagnetic Field Simulator*, http://www.gdfidl.de.

Burov, A., Lebedev, V. (2002). *Transverse Resistive Wall Impedance for Multi-Layer Flat Chambers*, EPAC 2002, Paris.

Byrd, J., Georgsson, M. (2001). Phys. Rev. ST-AB **4**, 030701 (2001).

Byrd, J. (2014). Harmonic RF Systems in Electron Storage Rings, talk given at TWIICE workshop, Synchrotron SOLEIL. *High factor of feedback gain against TMCI* reported at TWIICE.

Cai, Y. (2011). Proc. of IPAC2011, San Sebastian, Spain, 3775.

Cai, Y. et al. (2011). PEP-X: *An Ultimate Storage Ring based on Fourth-Order Geometric Achromats*, SLAC-PUB-14785, December 2011.

Caiafa, H. (2014). *Impedance Optimization and Wakefield Codes Comparison for the Brazilian Light Laboratory (LNLS/CNPEM)*, talk given at TWIICE workshop, Synchrotron SOLEIL.

Chao, A. W. (1993). *Physics of Collective Beam Instabilities in High Energy Accelerators*, John Wiley & Sons, Inc.

Chao, A., Heifets, S., Zotter, B. (2002). Phys. Rev. ST-AB **5**, 111001 (2002).

Chin, Y.H. (1988). *MOSES User's Guide*, CERN-LEP 88-05, 1988.

CST Microwave Studio, (2014). https://www.cst.com/Products/CSTMWS.

Eriksson, M. (2010). Private communication, MAXIV-SOLEIL collaboration.

Derbenev, Ya. et al. (1995). TESLA FEL-Report 1995-05.

Faltens, A., Laslett, L. J. (1973). Part. Accel. 4, 151.

Gluckstern, R. et al. (1992). *Coupling Impedance of Beam Pipes of General Cross Section*, CERN Report No. 92-25, 1992.

Hahn, M. (2014). Private communication, ESRF, Grenoble, France.

Harkay, K. et al. (2002). *A Preliminary Comparison of Beam Instabilities among ESRF, APS and SPring-8 X-Ray Storage Ring Light Sources*, EPAC 2002, 1505, Paris, France.

Henry, O., Napoly, O. (1995). Part. Acc. **35**, p. 235 (1991).

Herbeaux, C. (2014). Private communication, Synchrotron SOLEIL.

Hoffmann, A., Myers, S. (1980). *Beam Dynamics in a Double RF System*, CERN-ISR-TH-RF-80-26.

Karantzoulis, E. et al. (2003). Phys. Rev. ST-AB **6**, 030703 (2003).

Keil, E., Schnell, W. (1969). CERN Report ISR-TH-RF/69-48 (1969).

Kernel, P. (2000). *High Current Single Bunch Transverse Instabilities in Storage Ring Light Sources: A New Approach Highlighting a Post-Head-Tail Mechanism*, Dissertation, J. Fourier University, Grenoble, France, October 2000.

Kernel, P., Nagaoka, R., Revol, J.L., Besnier, G. (2000). *High Current Single Bunch Transverse Instabilities at the ESRF: A New Approach*, EPAC 2000, 1133, Vienna, Austria.

Klein, M. et al. (2013). *Study of Collective Beam Instabilities for the MAXIV 3 GeV Ring*, IPAC 2013, 1730, Shanghai, China.

Klein, M. et al. (2014). *Investigation of Transverse Beam Instabilities in the MAX IV 3 GeV Ring using the Multibunch Code mbtrack*, talk given at TWIICE workshop, Synchrotron SOLEIL.

Krinsky, S. (2005). *Simulation of Transverse Instabilities in the NSLS-II Storage Ring*, BNL-75019-2005-IR.

Kubo, K., Oide, K. (2001). Phys. Rev. ST-AB **4**, 124401.

Laclare, J.L. (1987). *Bunched Beam Coherent Instabilities*, CERN 87-03.

Lebasque, P. (2013). Preliminary Design Reports for the MAXIV MIK, unpublished.

Lee, E.P., Faltens, A., Laslett, L.J., Smith, L. (1983). IEEE Trans. Nucl. Sci. NS-30, No. **4**, 2502.

Limbourg, C. (1996). *Ultimate Brilliance of Storage Ring Based Synchrotron Radiation Facilities of the 3rd Generation. Potential of Storage Ring Based Sources in the Production of Short and Intense X-ray Pulses*, Dissertation, J. Fourier University, Grenoble, France, October 1966.

Mariette, C. et al. (2007). *Excitation Stripline for SOLEIL Fast Transverse Feedback*, DIPAC 2007, Venice, Italy.

Matsumoto, H. et al. (2006). *Experience with a Zero Impedance Vacuum Flange at He Super-Leak Temperatures for the ILC*, EPAC 2006, 753, Edinburgh, Scotland.

Morgan, A.F.D., Rehm, G. (2008). *Performance and Features of the DIAMOND TMBF System*, EPAC 2008, 3281, Genoa, Italy.

Murphy, J. B., Krinsky, S., Gluckstern, R. L. (1997). Particle Accelerators, 57, 9.

Nagaitsev, S. (2005). Phys. Rev. ST-AB **8**, 064403.

Nagaoka, R. et al (2002). *Incoherent Transverse Tune Shifts due to Resistive Low-Gap Chambers*, EPAC 2002, 1541, Paris, France.

Nagaoka, R. (2002). ESRF Internal Machine Report 05-02/Theory, July 2002.

Nagaoka, R. (2004). *Numerical Evaluation of Geometric Impedance for SOLEIL*, EPAC 2004, 2041, Lucern, Switzerland.

Nagaoka, R. (2004). *Study of Resistive-Wall Effects on SOLEIL*, EPAC 2004, 2038, Lucern, Switzerland.

Nagaoka, R. (2006). *Instability Studies using Evaluated Wake Fields and Comparison with Observations at SOLEIL*, EPAC 2006, 2847, Edinburgh, Scotland.

Nagaoka, R. et al. (2006). *Recent Studies of Geometric and Resistive-Wall Impedance at SOLEIL*, EPAC 2006, 2850, Edinburgh, Scotland.

Nagaoka, R. (2007). *Geometric Impedance of U20 Taper Revisited*, SOLEIL internal note, November 2007.

Nagaoka, R., Bartolini, R., Rowland, J. (2009). *Studies of Collective Effects in SOLEIL and DIAMOND using the Multiparticle Tracking Codes sbtrack and mbtrack*, PAC2009, 4637, Vancouver, Canada.

Nagaoka, R. et al. (2010). *Operational Status of the Transverse Bunch by Bunch Feedback System at SOLEIL*, IPAC 2010, 2746, Kyoto, Japan.

Nagaoka, R. et al. (2014). *Fast Beam-Ion Instability Arising from Local Outgassing*, talk given at TWIICE workshop, Synchrotron SOLEIL.

Nakamura, T., Kobayashi, K. (2005). *FPGA Based Bunch-by-Bunch Feedback Signal Processor*, ICALEPCA 2005, Geneva, Switzerland, and references therein.

Ng, K.Y., Bane, K. (2010). *Explicit Expressions of Impedances and Wake Functions*, FERMILAB-FN-0901-APC.

Nodvick, J., Saxon, D. (1954). Phys. Rev. 96 1, 180.

Oide, K. (1986). *SAD*, an optics program written by K. Oide et al. at KEK.

Oide, K., Yokoya, K. (1990). *Longitudinal Single-Bunch Instability in Electron Storage Rings*, KEK Preprint 90-10, April 1990 A.

Pedrozzi, M., et al. (2003). *SLS Operational Performance with Third Harmonic Superconducting System*, 11th Workshop on RF Superconductivity, Lübeck/Travemünder, Germany.

Piwinski, A. (1974). Proc. 9th Int. Conf. on High Energy Acc. p.405.

Piwinski, A. (1992). *Wake Fields and Ohmic Losses in Flat Vacuum Chambers*, DESY HERA 92-04.

Piwinski, A. (2006). In Handbook of Accelerator Physics, 3rd Printing, (New Jersey: World Scientific) p. 142.

Piwinski, A. (1999). *The Touschek effect in Strong Focusing Storage Rings*, DESY 98-179.

Plouviez, E. et al. (2008). *Bunch by Bunch Transverse Feedback Development at ESRF*, EPAC 2008, 3297, Genoa, Italy.

Podobedov, B. (2007). *Impedance Minimization by Nonlinear Tapering*, PAC07, Albuquerque, New Mexico.

Podobedov, B., Stupakov, G. (2013). Phys. Rev. ST Accel. Beams **16**, 024401.

Raubenheimer, T.O. (1994). Particle Accelerators **45**, 111.

Raubenheimer, T.O., Zimmermann, F., Phys. Rev. E52, 5487 (1995).

Revol, J.L. et al. (2000). *Comparison of Transverse Single Bunch Instabilities between the ESRF and ELETTRA*, EPAC 2000, 1170, Vienna, Austria.

Ries, M. et al. (2012). In Proc. of IPAC2012, New Orleans, LA, 3030.

Sacherer, F. (1976). *Transverse Bunched-Beam Instabilities*, CERN/PS/BR 76-21.

Satoh, K., Chin, Y.H. (1983). Nucl. Instr. Meth. **207** (1983) 309.

Schwinger, J. (1945). *On Radiation by Electrons in a Betatron*, transcribed by M. Furman, LBNL-39088, Jan. 1998.

Seraphim, R. (2014). Private communication, Sirius, LNLS, Campinas, Brazil.

Sirius (2013). *Sirius Design Report, version 02/2013*, LNLS, Campinas, Brazil.

Stupakov, G., Kotelnikov, I. A. (2003). Phys. Rev. ST Accel. Beams **6**, 034401.

Stupakov, G., Bane, K.L.F., Zagorodnov, I. (2007). Phys. Rev. ST Accel. Beams **10**, 054401.

Stupakov, G., Kotelnikov, I. A. (2009). Phys. Rev. ST Accel. Beams **12**, 104401.

Suzuki, T., Yokoya, K. (1982). Nucl. Instr. Meth. **203** (1982) 45.

Svandrlik, M. et al. (2003). *Performance of the 3rd Harmonic Superconducting Cavity at ELETTRA*, 11th Workshop on RF Superconductivity, Lübeck/Travemünder, Germany.

Tavares, P.F. (2014). *Option foreseen for MAXIV*, private communication, Lund, Sweden.

Venturini, M., Warnock, R., (2002). Phys. Rev. Lett. **89** 224802.

Vivoli, A., Martini, M. (2010). *Intra-Beam Scattering in the CLIC Damping Rings*, IPAC'10, Kyoto, Japan, p. 3557.

Wang, L. et al. (2013). Phys. Rev. ST Accel. Beams **16**, 104402.

Warnock, R., (1991). In Proc. of 4th Advanced ICFA Beam Dynamics Workshop, **151** (Tsukuba, Japan).

Warnock, R., Morton, P. (1990). Part. Accel. 25 113, SLAC-PUB-4562, March 1988.

Warnock, R., Ellison, J., (2000). SLAC-PUB-8404 (2000).

Warnock, R. et al. (2013). Proc. of PAC2013, Pasadena, CA, 219.

Wolski, A. (2009). *Space Charge, Intra-beam Scattering and Touschek Effects*, 4th International Accelerator School for Linear Colliders, Beijing, September 2009.

Xia, G., Ohmi, K., Elsen, E. (2008). Nucl. Instr. Meth. A **593** (2008) 183.

Xiao, A. (2013). *On-Axis Injection Scheme for Ultra-Low-Emittance Light Sources*, PAC2013, Pasadena, California.

Yokoya, K. (1990). *Impedance of Slowly Tapered Structure*, CERN-SL-90-88 (AP).

Yokoya, K. (1993). Part. Accel. **41** (1993) 221.

Zagorodnov, I., Weiland, T. (2005). Phys. Rev. ST Accel. Beams **8**, 042001.

Zhou, D. (2011). Japanese Journal of Appl. Phys. **51**, 016401.

Zisman, M.S. et al. (1986). *ZAP User's Manual*, Lawrence Berkeley Laboratory Report No. LBL-21270, December, 1986.

Zotter, B. (1969). CERN Yellow Report No. 69-15, 1969.

Zotter, B. W., Kheifets, S. A. 1998. *Impedances and Wakes in High-Energy Particle Accelerators*, World Scientific

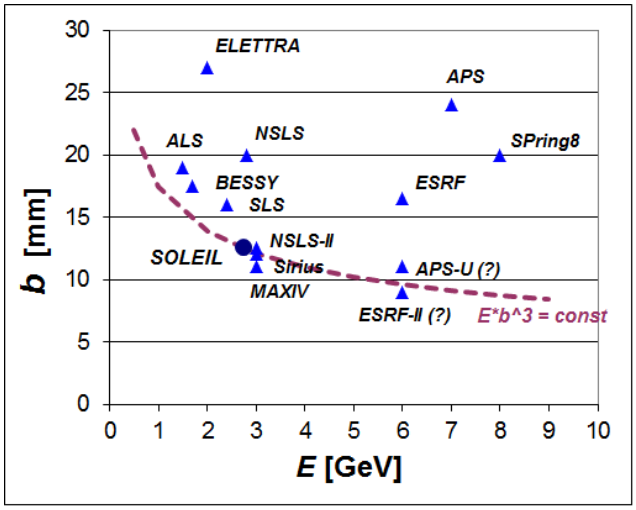

Figure 1

Half vertical aperture size of the standard vacuum chamber b versus energy E for several existing LSRs and DLSRs in construction or planned. The symbol (?) appearing for ESRF-II and APS-U signifies that the aperture values may still be re-optimized during the design stage (Hahn, 2014; Borland, 2014). The dashed curve represents a constant value of $E \cdot b^3$, adjusted to the SOLEIL case.

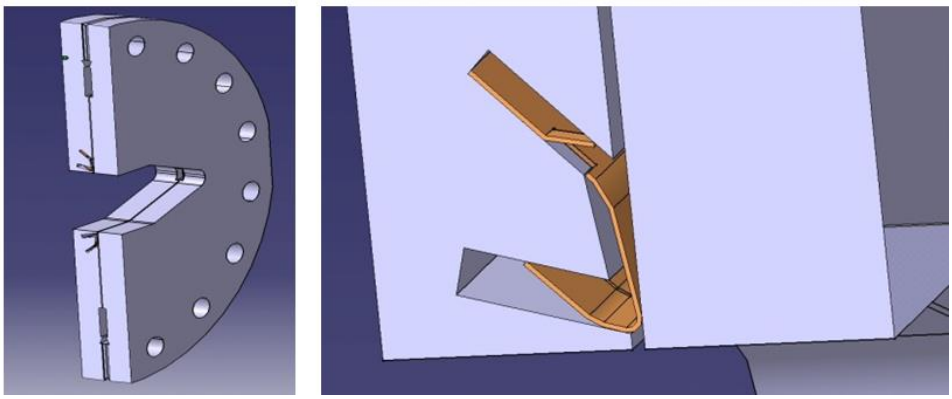

Figure 2

A short-circuited flange developed at SOLEIL. The metallic sheet (brown) inserted between the two plates effectively shields the 0.4 mm long and 50 mm deep cavity-like structure.

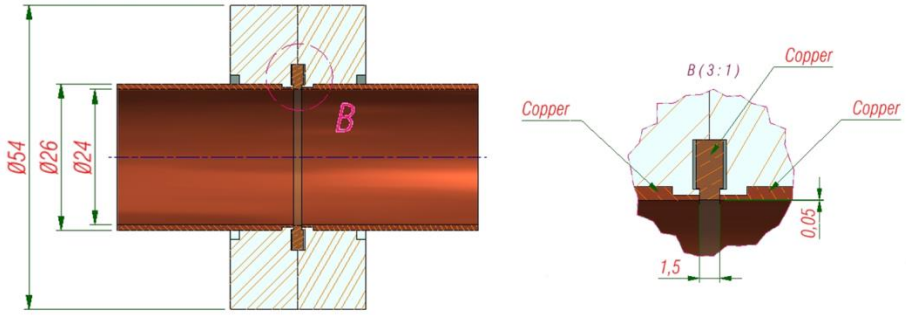

Figure 3

The "zero impedance" flange with no slit between the two plates developed at Sirius (Seraphim, 2014), on the basis of the model developed at KEK (Matsumoto *et al*., 2006). An additional effort is made so that an electron only sees copper in traversing a flange.

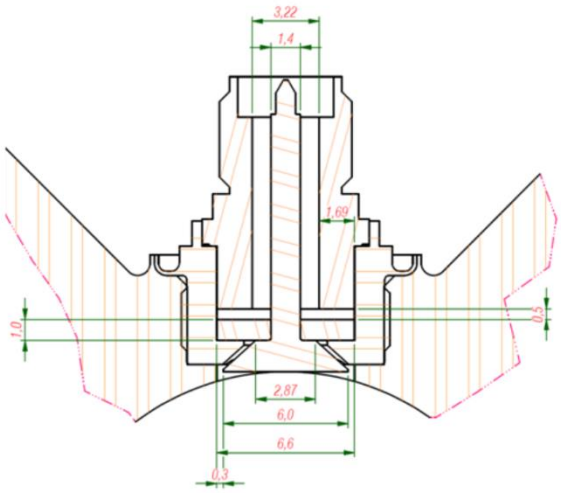

Figure 4

A bell shaped-BPM button design studied at Sirius (Caiafa, 2014). The shape is optimized to increase the button cut-off frequency without losing the button sensitivity, by keeping the bottom face area to a minimum value required.

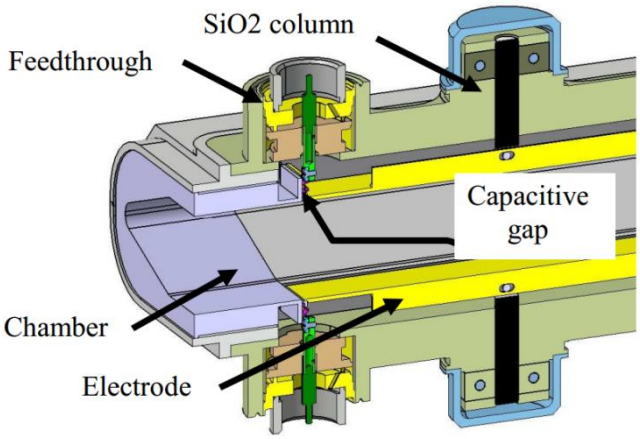

Figure 5

SOLEIL vertical stripline with its two electrodes embedded in the vacuum chamber without any transitions. The gap between the electrode and the chamber wall is 0.5 mm (Mariette *et al*., 2007).

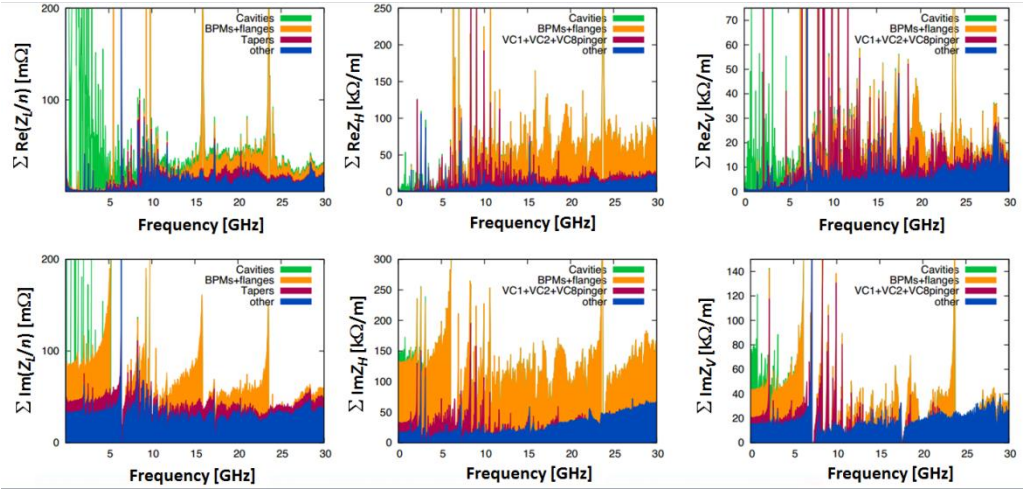

Figures 6

MAXIV 3 GeV ring geometric impedance budget, calculated with *GdfidL* in the longitudinal (left column), horizontal (central column) and vertical (right column) planes (Klein *et al*., 2013).

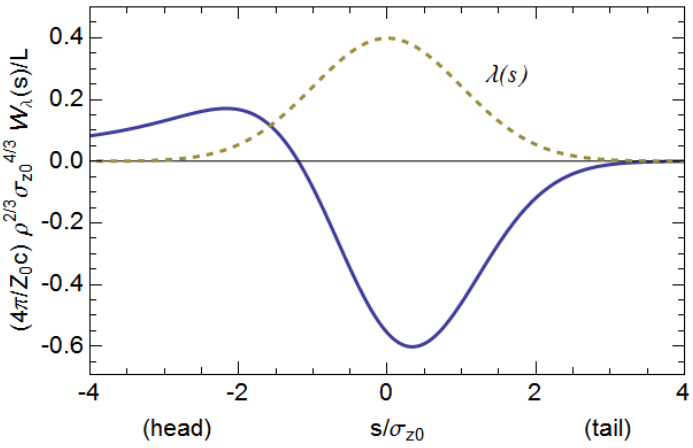

Figure 7

Bunch wake for a Gaussian bunch using the free space CSR model. The dashed curve gives the bunch shape with the head to the left. The loss factor $\kappa/L = 0.35(Z_0 c/4\pi)\rho^{-2/3}\sigma_{z0}^{-4/3}$.

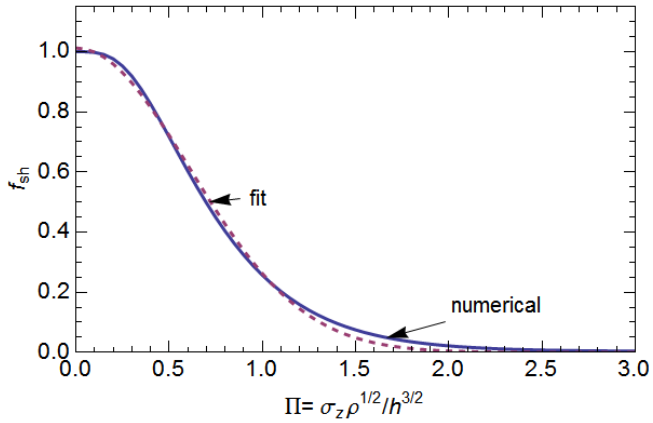

Figure 8

Factor $f_{sh} = \kappa_{sh}/\kappa_{free}$ vs. shielding parameter Π for Gaussian beam moving between conducting plains (from Bane, 2014). Shown are numerical results (blue) and the Gaussian fit $e^{-(\Pi/\sigma)^2/2}$, with σ = 0.609 (dashes).

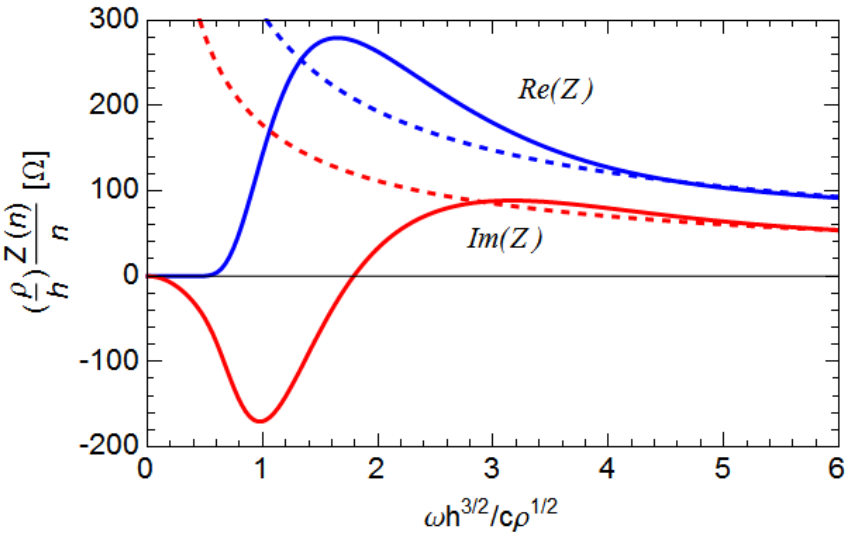

Figure 9

Scaled $Z(n)/n$ per turn, for CSR impedance with shielding and in free space (plot from Cai, 2011). $Re(Z)$ ($Im(Z)$) is given in blue (red). Y. Cai's shielded result is given by solid lines, and the free space impedance by dashes.

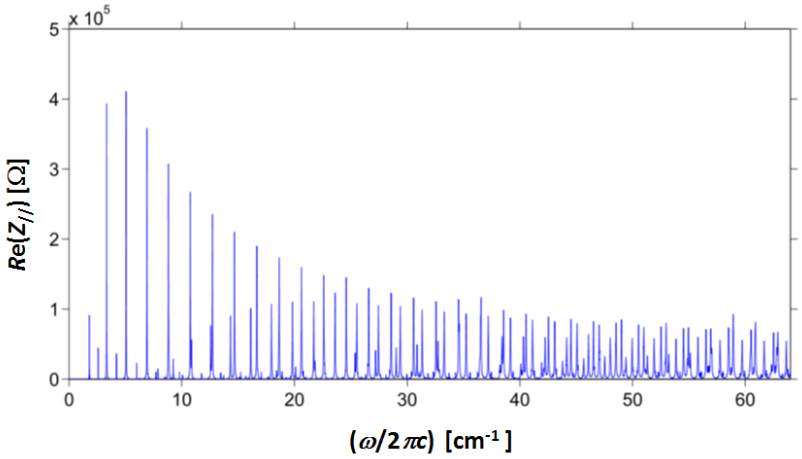

Figure 10

$Re(Z)$ in ohms for ANKA parameters, vs. $(\omega/2\pi c)$ in cm^{-1}. Here ρ = 5.6 m, height of the chamber h = 1.6 cm, and its width w = 6.8 cm (from Warnock *et al.*, 2013).

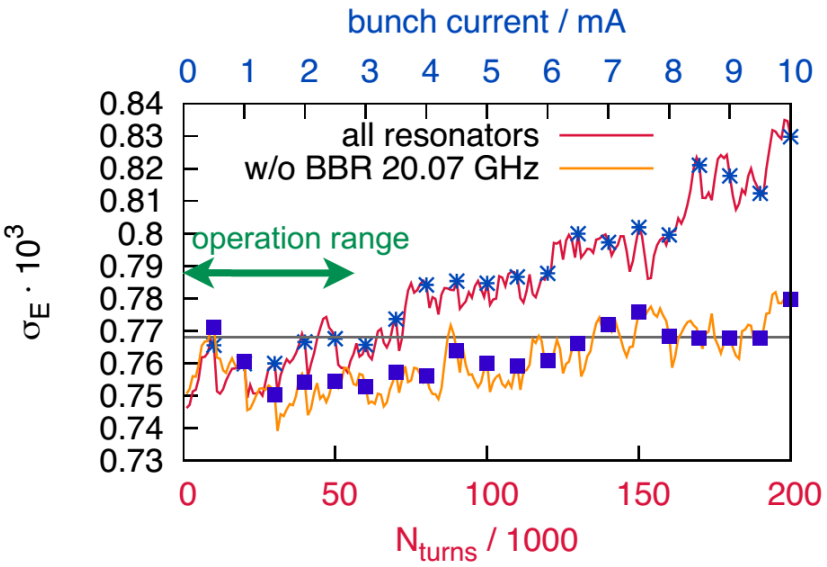

Figure 11

Energy spread σ_E versus single bunch current (the upper horizontal axis) calculated for MAXIV 3 GeV ring with *mbtrack* using the numerically obtained wake functions (Klein *et al.*, 2013). Note that the markers (stars and rectangles) indicate times when the beam current is increased by 0.5 mA at every 10000 turns. The gray horizontal line indicates the natural energy spread of 7.69×10^{-4}.

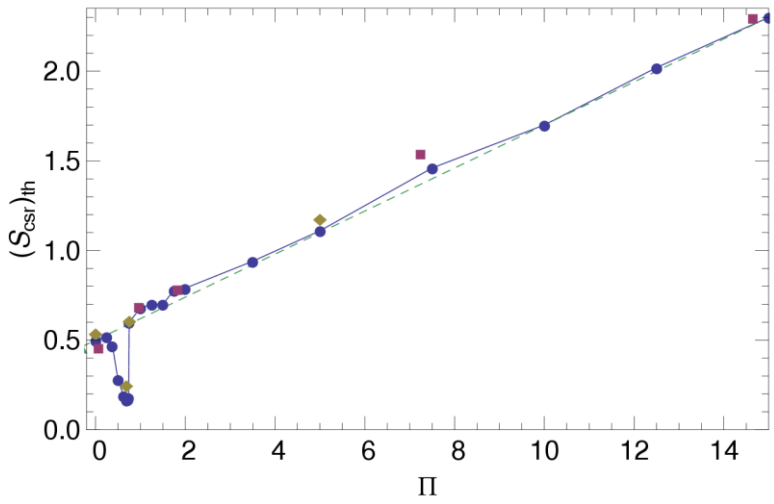

Figure 12

For the CSR wake, threshold value of $S_{csr} = I\rho^{1/3}/\sigma_{z0}^{4/3}$ vs. shielding parameter, $\Pi = \rho^{1/2}\sigma_{z0}/h^{3/2}$. Symbols give results of the VFP solver (blue circles), the LV code (red squares), and the VFP solver with twice stronger radiation damping (olive diamonds).

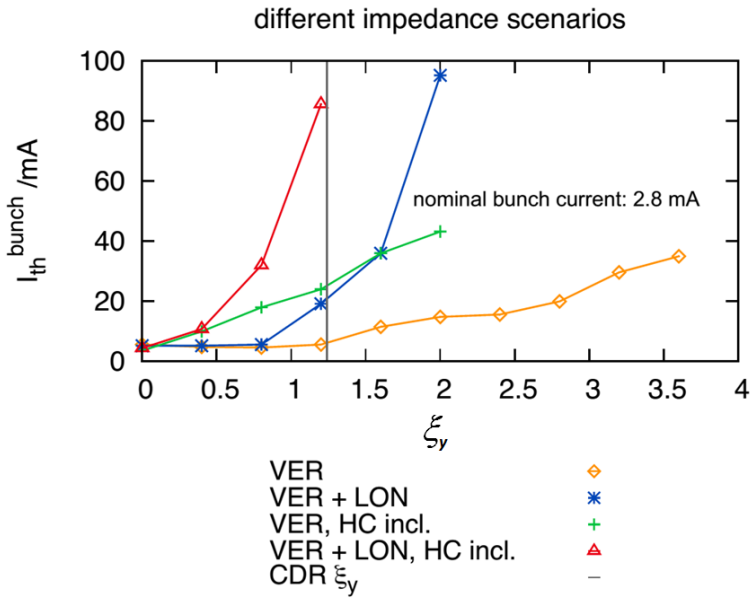

Figure 13

Vertical single bunch instability threshold versus single bunch current calculated for MAXIV 3 GeV ring with *mbtrack* using the numerically obtained wake functions (Klein *et al.*, 2013). VER: Vertical wakes. LON: Inclusion of longitudinal wakes in the longitudinal dynamics. HC incl.: Inclusion of Harmonic Cavities. CDR ξ_y: Value of chromaticity defined in the CDR report.

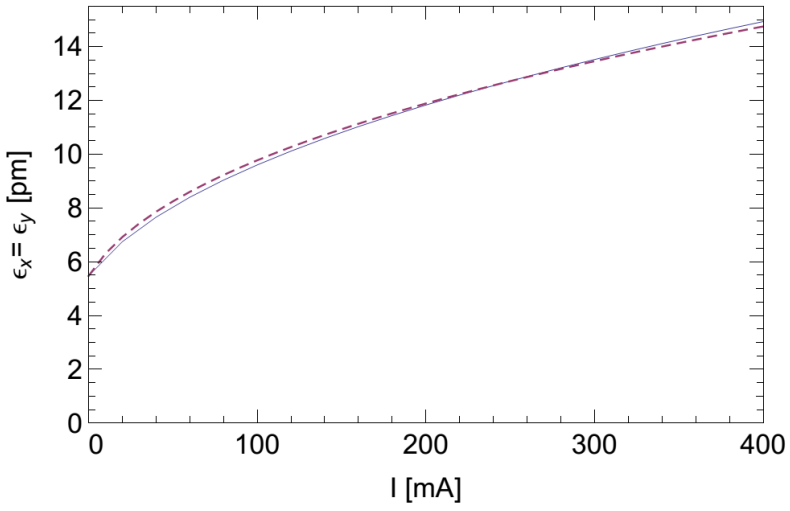

Figure 14

Steady-state emittances as function of bunch current in PEP-X.

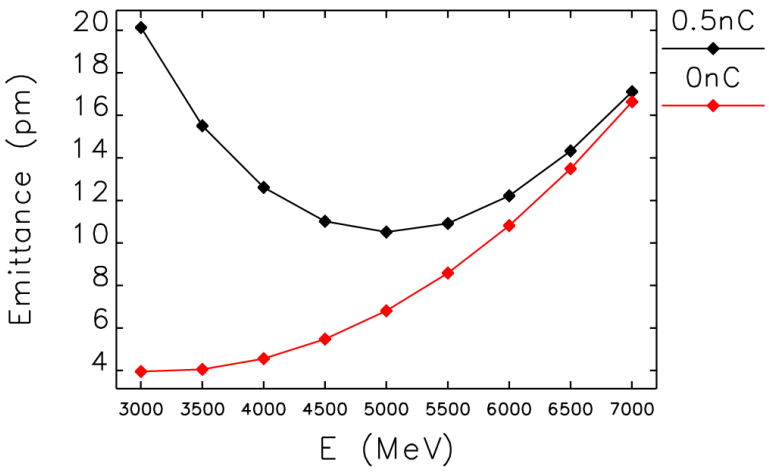

Figure 15

Emittance ε_x (= ε_y) vs. energy E for the PEP-X lattice at nominal (black) and at zero (red) currents (from Cai *et al*., 2011).

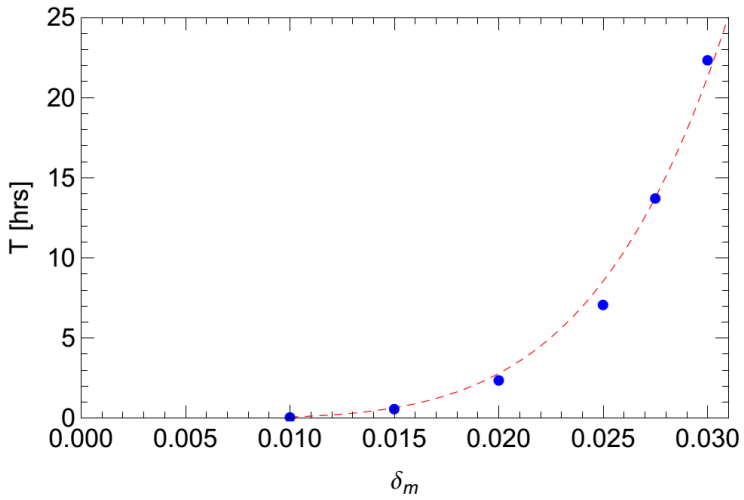

Figure 16

Touschek lifetime $\mathcal{T}$ for PEP-X vs. (global) momentum acceptance parameter, δ_m (blue symbols). The dashed curve gives the fit: $\mathcal{T} = 0.088(\delta_m/0.01)^5$ (from Cai *et al*., 2011).

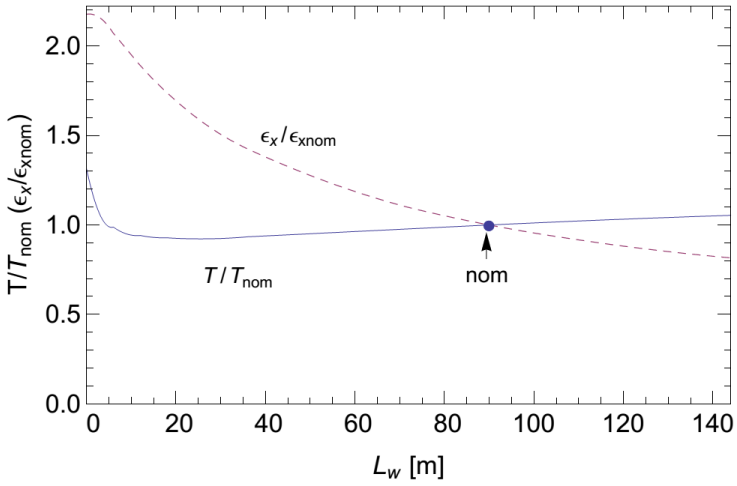

Figure 17

Emittance ε_x (= ε_y) and Touschek lifetime $\mathcal{T}$ vs. wiggler length L_ω. These results are self-consistent calculations including IBS. The points labeled "nom" represent the nominal case, with L_ω = 90 m (from Cai *et al.*, 2011).

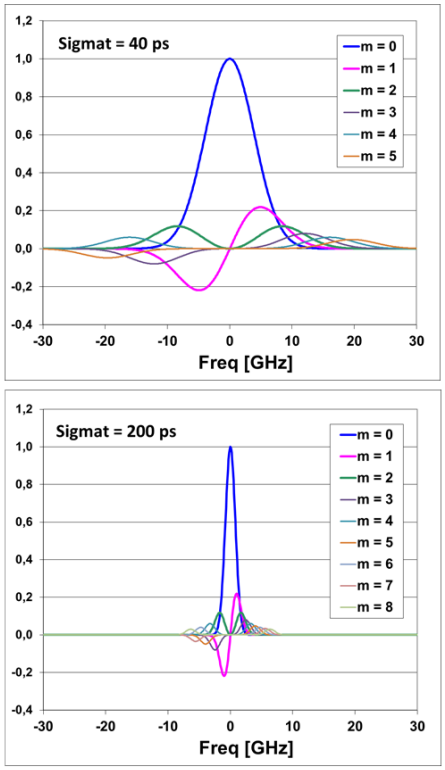

Figure 18

Distribution of head-tail mode spectra as a function of bunch length.